THE ASTROPHYSICAL JOURNAL, 518:2–23, 1999 June 10

COSMIC COMPLEMENTARITY: JOINT PARAMETER ESTIMATION FROM COSMIC MICROWAVE BACKGROUND EXPERIMENTS AND REDSHIFT SURVEYS

DANIEL J. EISENSTEIN, WAYNE HU,[1] AND MAX TEGMARK[2]
Institute for Advanced Study, Princeton, NJ 08540
Received 1998 July 2; accepted 1999 January 13

ABSTRACT

We study the ability of future cosmic microwave background anisotropy experiments and redshift surveys to constrain a 13-dimensional parameterization of the adiabatic cold dark matter model. Each alone is unable to determine all parameters to high accuracy. However, considered together, one data set resolves the difficulties of the other, allowing certain degenerate parameters to be determined with far greater precision. We treat in detail the degeneracies involving the classical cosmological parameters, massive neutrinos, tensor-scalar ratio, bias, and reionization optical depth as well as how redshift surveys can resolve them. We discuss the opportunities for internal and external consistency checks on these measurements. Previous papers on parameter estimation have generally treated smaller parameter spaces; in direct comparisons to these works, we tend to find weaker constraints and suggest numerical explanations for the discrepancies.

Subject headings: cosmic microwave background — cosmology: theory — dark matter — large-scale structure of universe — methods: numerical

1. INTRODUCTION

Current cosmological data have led astrophysicists to explore a structure formation paradigm in which cold dark matter driven by adiabatic fluctuations leads to the formation of galaxies and cosmic microwave background (CMB) anisotropies (see Blumenthal et al. 1984; Dodelson, Gates, & Turner 1996b for reviews). Experiments planned for the next decade will be able to test this paradigm more stringently by searching for distinctive features in the power spectra of CMB anisotropies and polarization (see Hu, Sugiyama, & Silk 1997 and Hu & White 1997b for reviews). If this framework is confirmed, then upcoming measurements, notably from the *MAP*[3] and *Planck*[4] satellites, will enable precision measurements of cosmological parameters such as the baryon fraction and matter-radiation ratio (Jungman et al. 1996a, 1996b; Zaldarriaga, Spergel, & Seljak 1997; Bond, Efstathiou, & Tegmark 1997; Copeland, Grivell, & Liddle 1998; Stompor & Efstathiou 1999).

As discussed by a number of authors, the details of the CMB power spectra contain a considerable amount of cosmological information. However, this leverage is not complete; altering the model parameters in particular combinations can yield power spectra that are observationally indistinguishable from a reference model (Bond et al. 1994, 1997; Zaldarriaga et al. 1997). The presence of these so-called degenerate directions means that a CMB data set will restrict the allowed models to a curve or surface in parameter space rather a point.

The galaxy power spectrum of large redshift surveys such as the 2dF survey[5] and the Sloan Digital Sky Survey (SDSS)[6] provide a different window on the cosmological parameter space. Taken alone, the results are again plagued by degeneracies (Tegmark 1997a; Goldberg & Strauss 1998; Hu, Eisentein, & Tegmark 1998a, hereafter HET). However, when combined with CMB data, the constraints can be highly complementary in that the degenerate directions of one lie along well-constrained directions for the other. A striking example involves the Hubble constant. By combining the data sets, features in the power spectrum can be measured in both real and redshift space, which allows the Hubble constant to be identified even though neither data set alone provides a good constraint (Eisenstein, Hu, & Tegmark 1998, hereafter EHT).

In this paper, we explore the details of how these data sets complement each other. In particular, we consider the constraints on cosmological parameters attainable by the statistical errors of this next generation of CMB experiments and redshift surveys. We identify physical mechanisms by which the data sets resolve degeneracies and explore them through progressions of cosmological models in the baryon fraction, neutrino mass, and tensor contribution. The combination of CMB data and large-scale structure has been studied with current data (Scott, Silk, & White 1995; Bond & Jaffe 1997; Lineweaver 1998; Gawiser & Silk 1998; Webster et al. 1998) as well as with future data in a smaller space of cosmological parameters but with more general initial conditions (Wang, Spergel, & Strauss 1999). We study how reducing the cosmological parameter space affects the degeneracies.

In addition to incorporating large-scale structure data, our treatment of parameter estimation in the case of CMB data alone uses the most general cosmology yet studied with both temperature and polarization information. Taking account of differences in cosmological parameterizations, fiducial models, and experimental specifications, we compare our results with past work in a series of tables. We generally find stronger degeneracies and hence weaker constraints than previous papers and propose numerical explanations for the discrepancies.

We review parameter estimation methods in § 2 and describe our parameterization of cosmology in § 3. We present a way of interpreting parameter covariance in

[1] Alfred P. Sloan Fellow.
[2] Hubble Fellow.
[3] http://map.gsfc.nasa.gov.
[4] http://astro.estec.esa.nl/SA-general/Projects/Planck.
[5] http://meteor.anu.edu.au/~colless/2dF.
[6] http://www.astro.princeton.edu/BBOOK/.

Appendix A and discuss the need for careful numerical treatments in Appendix B. In § 4, we compute the precision with which upcoming CMB experiments can potentially measure cosmological parameters. We compare our results to previous studies in Appendix C. In § 5, we add redshift survey information and conduct several parameter studies. We explore the dependence of our results on our assumptions in § 6. In § 7, we discuss the necessity of cosmological consistency checks and highlight a number of possibilities. We conclude in § 8.

2. FISHER MATRIX METHODS

The Fisher information matrix encodes the manner in which experimental data depends upon a set of underlying theoretical parameters that one wishes to measure (see Tegmark, Taylor, & Heavens 1997 for a review). Within this set of parameters, the Fisher matrix yields a lower limit to error bars and hence an upper limit on the information that can be extracted from such a data set. With the further assumptions of Gaussian-distributed signal and noise, Fisher matrices can be constructed from the specifications of both CMB experiments (Jungman et al. 1996b; Seljak 1996b; Zaldarriaga & Seljak 1997; Kamionkowski, Kosowsky, & Stebbins 1997) and redshift surveys (Tegmark 1997a). To the extent that the data sets are independent—a very good approximation for the cosmologies of interest—we can combine their constraints simply by summing their Fisher matrices.

Suppose that the observed data are written as $x_1, x_2, \ldots, x_n$, arranged as a vector $\boldsymbol{x}$. Then suppose that the model parameters are $p_1, p_2, \ldots, p_m$, arranged as a vector $\boldsymbol{p}$. Let the probability of observing a set of data $\boldsymbol{x}$ given the true parameters $\boldsymbol{p}$ (the "fiducial model") be $L(\boldsymbol{x}; \boldsymbol{p})$. The Fisher matrix is then defined as

$$\mathbf{F}_{ij} = -\left\langle \frac{\partial^2 \ln L}{\partial p_i \partial p_j} \right\rangle_{\boldsymbol{x}} . \tag{1}$$

The Cramér-Rao inequality says that the variance of an unbiased estimator of a parameter p_i from a data set cannot be less than $(\mathbf{F}^{-1})_{ii}$. In this sense, the Fisher matrix reveals the best possible statistical error bars achievable from an experiment.

Since the error bars on our independent variables $\boldsymbol{p}$ will in general be correlated, they do not contain sufficient information to calculate the errors on constructed quantities. A change of variables shows that the smallest possible variance on an unbiased estimator of some quantity $g(\boldsymbol{p})$ when marginalizing over the other directions that span the parameter space is

$$\text{Var}\ (g) = \sum_{i,j} \left(\frac{\partial g}{\partial p_i}\right) (\mathbf{F}^{-1})_{ij} \left(\frac{\partial g}{\partial p_j}\right) . \tag{2}$$

More generally, the Fisher matrix transforms as a tensor under a change of variables in parameter space. We will use equation (2) to quote errors for a number of these constructed quantities, such as σ_R, the rms mass fluctuations in a sphere of $R\,h^{-1}$ Mpc radius.

It is at times convenient to think of the inverse of the Fisher matrix as a covariance matrix with an associated error ellipsoid. This view can be misleading. First, it represents a degeneracy as a straight line rather than the true curve. For example, a CMB experiment might determine $\Omega_m h^2$ well but neither Ω_m nor h well. The proper error contour in the Ω_m-h plane would be a banana-shaped region along a curve of constant $\Omega_m h^2$; however, it will instead be represented as a long ellipse with the slope of the $\Omega_m h^2$ curve at the location of the fiducial model.

Second, the error contours from the Fisher matrix are not necessarily those that would be obtained from a likelihood or goodness-of-fit analysis of a particular data set. If the Fisher matrix errors are roughly constant across the error region itself (i.e., if the likelihood function is nearly Gaussian), then these various error bars will be comparable. This generally occurs when the error estimates are small compared to characteristic range over which a given cosmological parameter affects model predictions (Zaldarriaga et al. 1997). As we will see, this is usually the case when CMB and redshift surveys are combined, but CMB data alone are subject to degenerate directions that surely violate the approximation. In these cases, the question of what confidence region to use descends into the murky debate between frequentists and Bayesians. If a strong degeneracy is present, the Fisher matrix method is guaranteed to find it, but different methods may disagree on the size and shape of the error region. After this paper was submitted, a paper investigating this issue with Monte Carlo methods was submitted by Efstathiou & Bond (1999).

2.1. *CMB Anisotropies*

Under the assumption of Gaussian perturbations and Gaussian noise, the Fisher matrix for CMB anisotropies and polarization is (Seljak 1996b; Zaldarriaga & Seljak 1997; Kamionkowski et al. 1997)

$$\mathbf{F}_{ij} = \sum_{\ell} \sum_{X,Y} \frac{\partial C_{X\ell}}{\partial p_i} (\text{Cov}_\ell)^{-1}_{XY} \frac{\partial C_{X\ell}}{\partial p_j} , \tag{3}$$

where $C_{X\ell}$ is the power in the ℓth multipole for $X = T, E, B$, and C—the temperature, E-channel polarization, B-channel polarization, and temperature-polarization cross-correlation, respectively. We will use C_ℓ at times to refer to all the CMB power spectra together. The elements of the (symmetric) covariance matrix Cov_ℓ between the various power spectra are

$$(\text{Cov}_\ell)_{TT} = \frac{2}{(2\ell+1) f_{\text{sky}}} (C_{T\ell} + w_T^{-1} B_\ell^{-2})^2 , \tag{4}$$

$$(\text{Cov}_\ell)_{EE} = \frac{2}{(2\ell+1) f_{\text{sky}}} (C_{E\ell} + w_P^{-1} B_\ell^{-2})^2 , \tag{5}$$

$$(\text{Cov}_\ell)_{BB} = \frac{2}{(2\ell+1) f_{\text{sky}}} (C_{B\ell} + w_P^{-1} B_\ell^{-2})^2 , \tag{6}$$

$$(\text{Cov}_\ell)_{CC} = \frac{1}{(2\ell+1) f_{\text{sky}}} [C_{C\ell}^2 + (C_{T\ell} + w_T^{-1} B_\ell^{-2}) \times (C_{E\ell} + w_P^{-1} B_\ell^{-2})] , \tag{7}$$

$$(\text{Cov}_\ell)_{TE} = \frac{2}{(2\ell+1) f_{\text{sky}}} C_{C\ell}^2 , \tag{8}$$

$$(\text{Cov}_\ell)_{TC} = \frac{2}{(2\ell+1) f_{\text{sky}}} C_{C\ell} (C_{T\ell} + w_T^{-1} B_\ell^{-2}) , \tag{9}$$

$$(\text{Cov}_\ell)_{EC} = \frac{2}{(2\ell+1) f_{\text{sky}}} C_{C\ell} (C_{E\ell} + w_P^{-1} B_\ell^{-2}) , \tag{10}$$

$$(\text{Cov}_\ell)_{TB} = (\text{Cov}_\ell)_{EB} = (\text{Cov}_\ell)_{CB} = 0 . \tag{11}$$

Here B_ℓ^2 is the beam window function, assumed Gaussian with $B_\ell^2 = \exp\,[-\ell(\ell+1)\theta_{\rm beam}^2/8\ln 2]$, where $\theta_{\rm beam}$ is the full width, half-maximum (FWHM) of the beam in radians. w_T and w_P are the inverse square of the detector noise level on a steradian patch for temperature and polarization, respectively. A fully polarized detector has $w_P = 2w_T$. For multiple frequency channels, wB_ℓ^2 is replaced by the sum of this quantity for each channel. These formulae are derived in the $f_{\rm sky} = 1$ case; the approximation for $f_{\rm sky} < 1$ including sample variance (Scott, Srednicki, & White 1994) only gives the correct Fisher matrix provided that the power spectra have no sharp spectral features on scales $\Delta\ell \lesssim \Delta\theta^{-1}$, where $\Delta\theta$ is the angular extent of the map in the narrowest direction (Tegmark 1997b). Within the class of models we are considering, this should be an excellent approximation for *MAP* and *Planck* except at $l \lesssim 10$ where sample variance is large anyway.

We normalize the CMB power spectra to *COBE* when using equation (3) (Bunn & White 1997).

In Table 1, we list the experimental specifications for the *MAP* and *Planck* satellites used in this paper. We use $f_{\rm sky} = 0.65$ in all cases. We are not using the 22 GHz or 30 GHz channels of *MAP* and are using only two of the 10 channels of *Planck*. The rationale is that the statistical power of these channels will be used for multifrequency subtraction of foregrounds, leaving the full power of the remaining channels for cosmological use. We will discuss this further in § 6.1.

2.2. *Redshift Surveys*

For the power spectrum derived from galaxy redshift surveys, the Fisher matrix may be approximated as (Tegmark 1997a)

$$\mathbf{F}_{ij} = \int_{k_{\rm min}}^{k_{\rm max}} \frac{\partial \ln P(k)}{\partial p_i}\,\frac{\partial \ln P(k)}{\partial p_j}\,V_{\rm eff}(k)\,\frac{k^2 dk}{(2\pi)^2}\,, \qquad (12)$$

$$V_{\rm eff}(k) = \int \left[\frac{\bar{n}(\boldsymbol{r})P(k)}{1+\bar{n}(\boldsymbol{r})P(k)}\right]^2 d^3\boldsymbol{r}\,, \qquad (13)$$

where $\bar{n}(\boldsymbol{r})$ is the survey selection function, i.e., the expected number density of galaxies at the location $\boldsymbol{r}$. $P(k)$ is the model galaxy power spectrum. $V_{\rm eff}(k)$ is the effective volume of the survey, properly weighing the effects of shot noise in undersampled regions. $k_{\rm min}$ is the minimum wavenumber to which the survey is sensitive, but in practice the numerical results are virtually unchanged by taking $k_{\rm min} = 0$ since both $V_{\rm eff}$ and the phase-space factor k^2 vanish as $k \to 0$. $k_{\rm max}$ is the maximum wavenumber used for parameter estimation; we use 0.1 h Mpc^{-1} as a default but will discuss this at length.

TABLE 1

CMB Experimental Specifications

Experiment	Frequency	$\theta_{\rm beam}$	σ_T	σ_P
MAP	40	28.2	17.2	24.4
	60	21.0	30.0	42.6
	90	12.6	49.9	70.7
Planck	143	8.0	5.2	10.8
	217	5.5	11.7	24.3

Notes.—Frequencies in GHz. Beam size $\theta_{\rm beam}$ is the FWHM in arcminutes. Sensitivities σ_T and σ_P are in μK per FWHM beam (and hence C_ℓ must be in μK^2). $w = (\theta_{\rm beam}\,\sigma)^{-2}$ is the weight given to that channel.

Equation (12) was derived under the approximation that the galaxy distribution is that of a Gaussian random field and that the power spectrum has no features narrower than the inverse scale of the survey. It also neglects edge effects and redshift distortions. Fortunately, the SDSS is both wide angle (π steradians) and deep, so power spectrum features (e.g., baryonic oscillations) should be well resolved and edge effects manageable (Heavens & Taylor 1997; Tegmark et al. 1998b; cf. Kaiser & Peacock 1991). The 2dF survey, however, has a more complicated geometry and will require a more careful analysis.

We will quote our results for the Bright Red Galaxy (BRG) portion of the SDSS. This subsample will be intrinsically red galaxies; such galaxies tend to be bright cluster galaxies, and so the sample will reach significantly deeper than the primary survey. We assume the sample to be volume-limited with 10^5 galaxies to a depth of 1 Gpc and to have a bias such that $\sigma_{8,\rm gal} = 2$. We will also consider the results for the main SDSS, which includes 10^6 galaxies with a more complicated radial selection function; we assume this sample to have $\sigma_{8,\rm gal} = 1$. The value of $\sigma_{8,\rm gal}$ affects the normalization of $P(k)$ in equation (13); together with the assumed CMB normalization and spectral tilt, it implies that the fiducial model may have galaxy bias $b \neq 1$.

We will focus entirely on the power spectrum at large scales, where linear theory is expected to be a good approximation. We do this by choosing $k_{\rm max}$ to be roughly the scale at which nonlinear clustering becomes important (Tegmark 1997a). While data on smaller scales will yield very accurate measures of the power spectrum and higher order correlation functions, their interpretation in terms of cosmological parameters is much more complicated (Fry & Gaztañaga 1993; Peacock 1997; Mann, Peacock, & Heavens 1998). To be conservative, we are neglecting the cosmological information on nonlinear scales. SDSS should also reveal a wealth of information about redshift distortions (see, e.g., Hamilton 1997; Hatton & Cole 1998) on both linear and nonlinear scales; we will return to this in § 7.

We assume that the galaxy bias is linear on these large scales. This has some theoretical justification (Coles 1993; Fry & Gaztañaga 1993; Weinberg 1995; Scherrer & Weinberg 1998; Mann et al. 1998). More important, this assumption will be stringently tested by the SDSS and other large surveys. Galaxies of different morphologies or type will have different levels of bias, but linear bias predicts that the ratios of the various power spectra should be constant on large scales. Scale-dependent bias has been detected on small scales (Peacock 1997), but this does not test the linear bias assumption we are making here. In addition, redshift distortions may be able to probe any scale dependence of bias on large scales.

3. PARAMETERIZED COSMOLOGY

We adopt a 13-dimensional parameterization of the adiabatic CDM model. Our independent variables include the matter density $\Omega_m h^2$, the baryon density $\Omega_B h^2$, the massive neutrino density $\Omega_\nu h^2$, the cosmological constant Ω_Λ, and a curvature contribution Ω_K. Here, the Hubble constant is written as $H_0 \equiv 100\ h$ km s^{-1} Mpc^{-1}. These definitions imply that the total matter density in units of the critical density $\Omega_m \equiv 1 - \Omega_\Lambda - \Omega_K$, that the Hubble constant $h \equiv [(\Omega_m h^2)/\Omega_m]^{1/2}$, and that the CDM density $\Omega_{\rm CDM} h^2 \equiv \Omega_m h^2 - \Omega_B h^2 - \Omega_\nu h^2$. We use a single species of massive neutrinos, so the neutrino mass is $m_\nu \approx 94\Omega_\nu h^2$ eV (we take

units in which the speed of light is unity).

We include an unknown optical depth τ to reionization, implemented as a rapid and complete ionization event at the appropriate (small) redshift. We also allow the primordial helium fraction to vary but assume that the information from direct abundance measurements can be represented by a Gaussian prior $Y_p = 0.24 \pm 0.02$ (1 σ) (Bond et al. 1997; Schramm & Turner 1998).

We use an initial power spectrum of the form

$$P_\Phi = A_S^2 (k/k_{\rm fid})^{n_S(k)-4} \tag{14}$$

with

$$n_S(k) = n_S(k_{\rm fid}) + \alpha \ln (k/k_{\rm fid}) \tag{15}$$

for the fluctuations in the gravitational potential. Here, α is a logarithmic running of the tilt around a fiducial scale $k_{\rm fid} \equiv 0.025\ {\rm Mpc}^{-1}$. The density power spectrum is equal to the potential power spectrum times $(k^2 + 3\Omega_K H_0^2)^2$; the simplest open inflationary models predict a power law in the potential, not in the density. In a flat universe, the initial density power spectrum takes on the usual $A_S^2 (k/k_{\rm fid})^{n_S}$ form. The present-day density power spectrum $P(k)$ of course differs by the square of the transfer function.

Note that equivalent parameters for a different choice of $k_{\rm fid}$ could be mapped into the parameters of equation (14); hence the value of $k_{\rm fid}$ is immaterial. However, because of the running of the tilt, the value and hence the error bars on the tilt itself become scale dependent. We will quote values at both the Hubble wavenumber and at $k_{\rm fid}$. The errors on α are scale independent for the parameterization of equation (14). As shown in Appendix A, for a given experiment and fiducial model, there is a "pivot" wavenumber $k_{\rm pivot}$ for which the errors on $n_S(k_{\rm pivot})$ and α are uncorrelated and the errors on $n_S(k_{\rm pivot})$ are equal to the errors on n_S when α is held fixed. As one might expect, $k_{\rm pivot}$ falls near the center of the observable range of wavenumbers, generally not too far from our choice of $k_{\rm fid}$. At other wavenumbers, the uncertainties on $n_S(k)$ are larger and correlated with α.

We allow tensor perturbations with a normalization T/S equal to the ratio of the $\ell = 2$ temperature anisotropies of the tensors and scalars. Note that this is proportional but not equal to the ratio A_T^2/A_S^2 that enters into the inflationary constraints. In particular, cosmological parameters enter into T/S owing to the evolution of quadrupole anisotropies (Knox 1995; Turner & White 1996). We parameterize the power-law exponent of the tensor input spectrum as n_T; this allows us to probe whether these data sets can test the inflationary consistency relation. However, for fiducial models with $T/S = 0$, excursions in n_T occur at $T/S = 0$, thereby yielding a zero derivative. Hence, in this limit, n_T is not a physically meaningful parameter and our parameter space is effectively reduced to 12 dimensions.

Finally, we allow the scalar normalization to vary and include an unknown linear bias. We describe our normalization choice in § B2.2; this choice can affect individual derivatives but does not affect marginalized errors. The linear bias b is defined by $P_{\rm gal} = b^2 P_{\rm mass}$. We also quote results for $\beta \equiv \Omega_m^{0.6}/b$ to facilitate comparisons to results from peculiar velocity data (Peebles 1980).

We discuss numerical issues involved with constructing derivatives with respect to these parameters in Appendix B. Here we simply note that our results in Table 2 are stable to 10% when step sizes are halved and that we have spot-checked elsewhere with similar results. Stability improves as parameter degeneracies are removed, either by the addition of other data sets or by external priors.

TABLE 2

MARGINALIZED ERRORS FOR ΛCDM FOR VARIOUS CMB EXPERIMENTS

	CMB ALONE					CMB+SDSS			
	MAP		*Planck*			*MAP*		*Planck*	
QUANTITY	Temp	T+P	Temp	T+P	SDSS ALONE	Temp	T+P	Temp	T+P
h	1.3	0.22	1.1	0.13	1.3	0.030	0.029	0.025	0.022
Ω_m	1.4	0.24	1.2	0.14	0.23	0.042	0.036	0.035	0.027
$\Omega_m h$	0.47	0.078	0.40	0.046	0.59	0.024	0.018	0.015	0.010
Ω_Λ	1.1	0.19	0.96	0.11	∞	0.056	0.042	0.036	0.024
Ω_K	0.31	0.055	0.26	0.030	∞	0.022	0.015	0.007	0.005
$\ln(\Omega_m h^2)$	0.20	0.095	0.064	0.018	4.5	0.11	0.077	0.040	0.016
$\ln(\Omega_B h^2)$	0.13	0.060	0.035	0.010	5.6	0.074	0.050	0.026	0.010
$m_\nu\ (eV) \propto \Omega_\nu h^2$	0.89	0.58	0.58	0.26	9.1	0.38	0.33	0.31	0.21
Y_P	0.020	0.020	0.018	0.013	...	0.020	0.020	0.017	0.013
$n_S(k_{\rm fid})$	0.11	0.048	0.041	0.008	1.1	0.064	0.040	0.028	0.008
$n_S(H_0)$	0.32	0.17	0.18	0.039	4.1	0.23	0.14	0.13	0.038
α	0.030	0.018	0.015	0.004	0.42	0.022	0.015	0.011	0.004
$\ln P_\Phi(k_{\rm fid}) \equiv \ln A_S^2$	1.4	0.43	1.1	0.073	∞	0.61	0.36	0.36	0.069
$\ln P_\Phi(H_0)$	1.8	0.71	1.3	0.16	∞	0.91	0.61	0.55	0.15
T/S	0.48	0.18	0.35	0.012	...	0.24	0.16	0.15	0.012
τ	0.69	0.022	0.59	0.004	...	0.27	0.021	0.21	0.004
$\ln \sigma_8$	0.48	0.14	0.42	0.057	∞	0.27	0.070	0.22	0.044
$\ln(\sigma_{50}/\sigma_8)$	0.86	0.15	0.75	0.093	0.27	0.029	0.028	0.024	0.020
$\ln \beta$	...	...	...	...	∞	0.27	0.068	0.20	0.027
$\ln b$	...	...	...	...	∞	0.28	0.087	0.23	0.062

NOTES.—$\Omega_m = 0.35$, $\Omega_B = 0.05$, $\Omega_\nu = 0.0175$ ($m_\nu = 0.7$ eV), $\Omega_\Lambda = 0.65$, $h = 0.65$, $n_S = 1$, $\alpha = 0$, $\tau = 0.05$, $Y_p = 0.24$, and $T/S = 0$. $n_T = 0$ and cannot vary. All errors are 1 σ. $k_{\rm max} = 0.1\ h\ {\rm Mpc}^{-1}$. Blank entries indicate that the parameter does not affect the observables for the data set. Infinite entries indicate that the parameter affects observables but is not constrained owing to degeneracies; in particular, the growth factor, normalization, and bias are all degenerate.

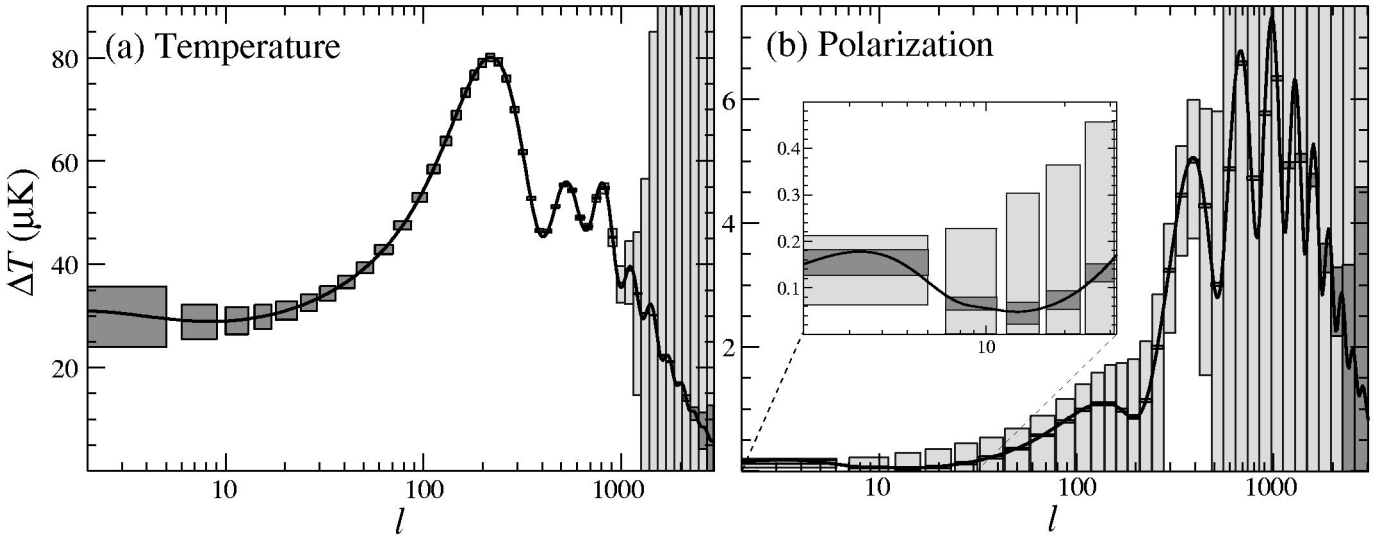

FIG. 1.—Our most used model along with 1 σ band-power error bars from *MAP* and *Planck*. The model is $\Omega_m = 0.35$, $h = 0.65$, $\Omega_B = 0.05$, $\Omega_\Lambda = 0.65$, $\Omega_\nu = 0.0175$, $\tau = 0.05$, $n_S(k_{\rm fid}) = 1$, and $T/S = \alpha = 0$. (*a*) The temperature power spectrum $\Delta T = [\ell(\ell+1)C_{T\ell}/2\pi]^{1/2}$. (*b*) The *E*-channel polarization power spectrum $\Delta T = [\ell(\ell+1)C_{E\ell}/2\pi]^{1/2}$; the panel shows a blow-up of the large-angle feature caused by reionization. *MAP* errors are the lighter, larger boxes; *Planck* errors are the darker, smaller boxes. The bands reflect an averaging over many ℓ; the actual experiments will have finer ℓ resolution (and correspondingly larger errors). *MAP* will be able to average the polarization bands together to get a marginal detection at $\ell \approx 150$, but *Planck* can trace out the full curve. Note that because polarization and temperature are correlated, the significance of detecting a change in parameters using both data sets is not simply given by the combination of errors from each.

3.1. *Fiducial Models*

The Fisher matrix formalism asks how well an experiment can distinguish the true ("fiducial") model of the universe from other models. The results clearly depend upon the fiducial model itself. We will quote results for a number of models, but most of our studies are based around a low-density, geometrically flat ΛCDM model with $\Omega_m = 0.35$, $h = 0.65$, $\Omega_B = 0.05$, $\Omega_\Lambda = 0.65$, $\Omega_\nu = 0.0175$ ($m_\nu = 0.7$ eV), $\tau = 0.05$, $n_S(k_{\rm fid}) = 1$, and $T/S = 0$, in the region of parameter space favored by recent data. We display the CMB and matter power spectra for this model in Figures 1 and 2. Note that although our fiducial model is flat, we do not restrict our excursions to flat models: we vary all 12 parameters (including Ω_K) simultaneously unless explicitly stating otherwise. Numerical issues are the reason for the small but nonzero values of Ω_ν and τ here (see Appendix B). We will alter the fiducial values of Ω_B, Ω_ν, and T/S in various parameter studies. In § 5.3, we will consider an $\Omega_m = 1$ SCDM model, a $\Omega_m = 0.35$ open CDM model, and a $\Omega_m = 0.2$ flat model. $Y_p = 0.24$, $\tau = 0.05$, $\alpha = 0$, and $n_T = 0$ in all models.

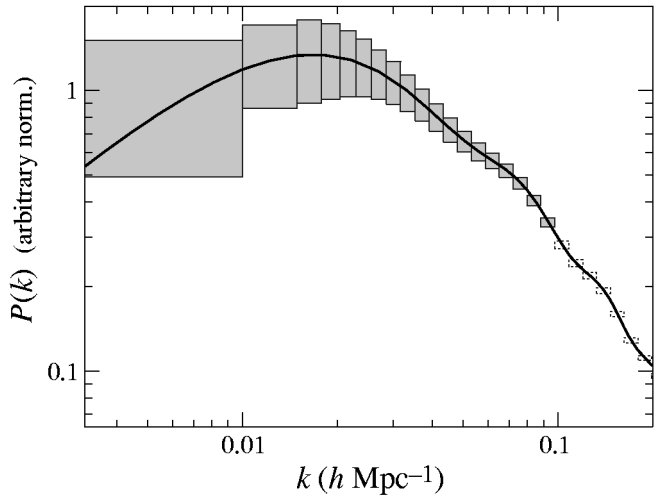

FIG. 2.—Power spectrum for the model of Fig. 1. SDSS BRG 1 σ error bars are superposed. Dashed boxes are for $k > k_{\rm max} = 0.1\ h\ {\rm Mpc}^{-1}$; we neglect information from these scales unless otherwise noted. Note the acoustic oscillations in the power spectrum, e.g., the bump at $k = 0.08\ h\ {\rm Mpc}^{-1}$; see § 5.2 for further discussion.

4. CMB ALONE

We begin by presenting the constraints that could in principle be achieved by CMB satellites without galaxy power spectrum information. Table 2 shows the results on a variety of quantities using a $\Omega_m = 0.35$, $\Omega_\Lambda = 0.65$ CDM model as our fiducial model. As expected, CMB data alone provide excellent constraints on $\Omega_B h^2$, $\Omega_m h^2$, $n_S(k_{\rm fid})$, and α, as well as on a combination of Ω_K and Ω_Λ. The last of these occurs because the angular scale of the acoustic features requires a particular value of the angular diameter distance to the last scattering surface. Note that $\Omega_m h^2$ and $\Omega_B h^2$ are simply the comoving densities of matter and baryons, respectively. With polarization information, the CMB also strongly constrains the reionization optical depth τ.

However, the remaining parameters are nowhere near "percent level" in accuracy, even for *Planck*. This is because of various degeneracies, particularly the angular diameter distance degeneracy and the reionization-normalization degeneracy. Although these were discussed in previous papers, none of the tables in Jungman et al. (1996b), Zaldarriaga et al. (1997), Bond et al. (1997), or Copeland et al. (1998) include the case where Ω_K and Ω_Λ are measured simultaneously. As is well known, at fixed $\Omega_m h^2$ and $\Omega_B h^2$, the morphology of the acoustic peaks is independent of the value of Ω_Λ and Ω_K. Choosing the combination of changes in Ω_Λ and Ω_K that holds constant the angular diameter

distance to the last scattering epoch then keeps the angular location and shape of the acoustic peaks fixed, which implies that Ω_Λ and Ω_K are strongly degenerate. This ambiguity causes the value of h, Ω_m, and $\Omega_m h$ to be poorly constrained (EHT); moreover, these uncertainties propagate into the rms density fluctuations σ_R owing to the redshift-space definition of the top-hat radius R (h^{-1} Mpc). Any additional parameter that affects the angular diameter distance relation, e.g., variations in the equation of state of the missing energy, creates a similar degeneracy. The severity of the degeneracy requires a careful numerical treatment, which we describe in Appendix B2.

Adding polarization information to the CMB helps for most quantities. Much of the improvement comes from the ability of polarization information to isolate reionization and tensor contributions (Zaldarriaga et al. 1997), thereby separating the large-angle temperature effects of Ω_Λ and Ω_K. Table 2 illustrates that removing this ambiguity substantially reduces errors on other quantities even with the polarization sensitivity of *MAP*.

Because the temperature-polarization correlation is not complete, polarization also provides independent information on the high-redshift, degree-scale acoustic oscillations to combat sample variance. This is best illustrated by fixing τ, T/S, and Ω_K, thereby eliminating the need to employ the large-angle polarization signal to break degeneracies. For the model in Table 2, adding polarization information to the temperature data in this restricted parameter set improves errors on $\Omega_m h^2$, $\Omega_B h^2$, Ω_Λ, and $n_S(k_{\rm fid})$ by about 40%–70% for *Planck*. The improvement is only 8% for *MAP*, so polarization maps of this sensitivity are useful only through their constraints on τ and T/S as discussed above.

Parameter estimation with the CMB alone has been discussed in the past in smaller parameter spaces and/or without polarization information. As discussed in Appendix C, our results disagree with several studies in the literature, generally by giving larger error bars.

5. COMPLEMENTARITY

5.1. *Adding Redshift Survey Data*

The addition of information on the matter power spectrum at the precision available within the SDSS can make a substantial improvement in the error bars on key cosmological quantities. As seen in Table 2, one gets large improvements on h, Ω_m, and the related quantities $\Omega_m h$, Ω_Λ, and Ω_K, and moderate improvements in other quantities, particularly $\Omega_\nu h^2$. Of course, as one improves the quality of the CMB data set, the fixed level of SDSS input gets less and less important.

The most striking improvement allowed by measurement of the matter power spectrum is the breaking of the angular diameter distance degeneracy. Since Ω_Λ and Ω_K shift the acoustic peaks in opposite directions, to trade one off the other requires substantial changes in $\Omega_m = 1 - \Omega_\Lambda - \Omega_K$. Because this variation must be done at fixed $\Omega_m h^2$ to maintain the peak morphology, h varies strongly in the degenerate direction. A measurement of h thereby breaks the degeneracy.

The combination of CMB and galaxy survey data can do just that. Once $\Omega_m h^2$ and $\Omega_B h^2$ are well determined by the CMB acoustic peak morphology, the real-space power spectrum is known. Varying h causes this pattern to move in redshift space. Hence, the more features that are present in the matter power spectrum, the more accurately one can measure h and so break the degeneracy.

Within the types of CDM models considered here, the best source of power spectrum features is the oscillations impressed by baryonic oscillations. As shown in EHT and § 5.2, even a 10% baryon fraction causes large enough features for SDSS to clamp down on h and Ω_m. Indeed, the resulting error bars are nearly as good as if the universe were *assumed* flat in many cases, thereby breaking the degeneracy by fiat.

In other sectors, the gains are more modest. Improvements approaching a factor of 2 are possible in $\Omega_m h^2$ and $n_S(k_{\rm fid})$, particularly for *MAP* without polarization. Polarization tends to allow the CMB to dominate the constraints, but this does depend on the value of $k_{\rm max}$ and on being able to extract low-ℓ cosmological information. An important complementary aspect of the data sets enables the determination of the mass of cosmological neutrinos (HET). We will discuss this further in § 5.4.

As shown in Table 2, SDSS power spectrum information alone flounders in this large parameter space. Details of the shape do depend on cosmology, but the features are not well enough detected for this low baryon fraction and small $k_{\rm max}$ (see Fig. 2).

In all cases, the improvements depend somewhat on the value of $k_{\rm max}$, which we will vary in § 6.3. Reverting from the deeper BRG survey to the SDSS main survey degrades the performance on h and related quantities by about 30%.

5.2. *The Role of Baryons*

Table 3 shows the results as a function of the baryon fraction. As the baryon fraction increases, the addition of SDSS information becomes more and more helpful. h and the related quantities Ω_m, Ω_Λ, Ω_K, and σ_8 are the most affected, but even traditional CMB quantities such as $\Omega_m h^2$ or $\Omega_B h^2$ see marked improvement at high Ω_B/Ω_m.

The driving physical effect behind these gains is the structure that develops in the matter power spectrum owing to the high-redshift acoustic oscillations imprinted by a nonnegligible baryon fraction (Peebles & Yu 1970; Sunyaev & Zeldovich 1970; Holtzman 1989; Hu & Sugiyama 1996; Eisenstein & Hu 1998). In CDM cosmologies, the baryons and photons oscillate on subhorizon scales prior to recombination, while the CDM perturbations simply grow. The event of recombination catches the oscillations at various phases and creates the acoustic peaks we see in the CMB spectrum. The perturbations in the baryons also share this oscillatory history, but in trace-baryon cosmologies, it is erased as the baryons fall into the more evolved CDM perturbations. When the baryon fraction is nonnegligible, however, the equilibration of the baryon and CDM perturbations is not completely one-sided, and the final power spectrum $P(k)$ retains an imprint of the acoustic oscillations. The resulting morphology consists of a sharp break in the power spectrum followed by a damped series of wiggles; the whole pattern has a characteristic scale, known as the sound horizon, which is the distance a sound wave could travel prior to recombination. Figure 2 gives an illustration of this behavior.

As discussed in EHT, once CMB data yield $\Omega_m h^2$ and $\Omega_B h^2$, the physical size of the sound horizon is known. Measuring this scale in a redshift survey thereby allows a comparison that gives the Hubble constant. Once the baryon

TABLE 3

MARGINALIZED ERRORS AS FUNCTION OF Ω_B

	$\Omega_B = 0.005$		$\Omega_B = 0.02$		$\Omega_B = 0.05$		$\Omega_B = 0.10$	
QUANTITY	*MAP*	+SDSS	*MAP*	+SDSS	*MAP*	+SDSS	*MAP*	+SDSS
h	0.34	0.12	0.27	0.091	0.22	0.029	0.23	0.013
Ω_m	0.36	0.12	0.29	0.086	0.24	0.036	0.25	0.018
$\Omega_m h$	0.12	0.039	0.093	0.029	0.078	0.018	0.084	0.009
Ω_Λ	0.28	0.098	0.23	0.070	0.19	0.042	0.20	0.022
Ω_K	0.082	0.029	0.065	0.027	0.055	0.015	0.056	0.008
$\ln(\Omega_m h^2)$	0.091	0.089	0.11	0.101	0.095	0.077	0.073	0.034
$\ln(\Omega_B h^2)$	0.068	0.057	0.051	0.046	0.060	0.050	0.062	0.034
$m_\nu\ (eV) \propto \Omega_\nu h^2$	0.60	0.55	0.60	0.46	0.58	0.33	0.74	0.23
$n_S(k_{\rm fid})$	0.046	0.042	0.031	0.030	0.048	0.040	0.055	0.027
α	0.032	0.020	0.023	0.017	0.018	0.015	0.026	0.015
$\ln P_\Phi(k_{\rm fid}) \equiv \ln A_S^2$	0.39	0.35	0.30	0.28	0.43	0.36	0.47	0.23
T/S	0.11	0.11	0.15	0.14	0.18	0.16	0.17	0.13
τ	0.036	0.033	0.026	0.024	0.022	0.021	0.022	0.020
$\ln \sigma_8$	0.19	0.17	0.20	0.14	0.14	0.070	0.14	0.046
$\ln(\sigma_{50}/\sigma_8)$	0.27	0.031	0.19	0.026	0.15	0.028	0.13	0.026
$\ln \beta$	...	0.074	...	0.069	...	0.068	...	0.050
$\ln b$	...	0.31	...	0.23	...	0.087	...	0.046

NOTES.—Same ΛCDM model as Table 2, save for variations in Ω_B. Recall that $\Omega_m = 0.35$. $n_T = 0$ and cannot vary. All errors are 1 σ. CMB data are for *MAP* with temperature and polarization information. SDSS column uses information up to $k_{\rm max} = 0.1\ h\ {\rm Mpc}^{-1}$ as well as CMB data.

fraction is about 10% or greater, SDSS can detect the baryonic features and thereby collapse the error bars on h and related quantities.

In Table 3, the case of negligible baryons $\Omega_B = 0.005$ allows SDSS to make modest improvements over *MAP* alone. The factor of 3 improvement on h and Ω_m comes from the two scales that remain as Ω_B becomes small: the scale of the horizon at matter-radiation equality, which is proportional to $\Omega_m h$, and the scale of the horizon when the massive neutrinos become nonrelativistic. The latter is a result of using a 5% neutrino fraction; the former is always present but is imprecisely measured due to confusion with spectral tilt.

Baryon fractions exceeding 10% are strongly favored by observations of cluster X-ray gas (White, Efstathiou, & Frenk 1993a; David, Jones, & Forman 1995; White & Fabian 1995; Evrard 1997). Lyα forest theories also favor high baryon densities (Weinberg et al. 1997); when combined with the general observational preference for low matter densities (see, e.g., Bahcall, Fan, & Cen 1997; Carlberg et al. 1997a; Carlberg, Yee, & Ellingson 1997b), this yields a high baryon fraction. Hence, it seems likely that baryonic features will be prominent enough in the matter power spectrum that SDSS, and perhaps 2dF will be able to detect them (Tegmark 1997a; Goldberg & Strauss 1998).

If the baryon fraction is yet higher, perhaps 20%, then the detailed morphology of the baryon features can be studied well enough to tighten constraints on other, non–h-related, parameters. The final columns in Table 3 show that a baryon fraction of 28% could allow SDSS to make a factor of 2 improvement in $\Omega_m h^2$, $\Omega_B h^2$, and $n_S(k_{\rm fid})$ over *MAP* with polarization.

5.3. *Variations in Ω_m and Ω_K*

We show the marginalized errors for three other choices of Ω_m and Ω_K in Table 4. The results are similar to those of the previous sections, with some expected variations. Performance with SDSS on h and Ω_m is worse (better) in the $\Omega_m = 1$ SCDM ($\Omega_m = 0.2$ ΛCDM) model because the baryonic oscillations in the matter power spectrum get horizontally shifted to less (more) favorable locations relative to the fixed cutoff scale of $k_{\rm max} = 0.1\ h\ {\rm Mpc}^{-1}$. On the other hand, the degree of nonlinearity at that scale is not fixed. Abundances of rich clusters require that low-Ω_m cosmologies have a higher σ_8 than high-Ω_m cosmologies (White et al. 1993b; Viana & Liddle 1996; Eke, Cole, & Frenk 1996; Pen 1998); this suggests that a given level of nonlinearity should occur at high values of k in higher Ω_m cases. In other words, had we fixed $k_{\rm max}$ by requiring that cluster-normalized fluctuations reach a particular amplitude on that scale, the number of baryon oscillations in the linear regime, and hence the performance of SDSS, would have remained more constant.

As expected, the $\Omega_m = 0.35$ open cosmology does show somewhat worse performance than its flat cousin for *MAP* data, presumably because the acoustic peaks have been shifted to smaller scales, leaving less structure to be resolved by the beam. This effect is smaller for *Planck*—while fewer peaks are detected, the sample-variance errors on scales around the sound horizon are improved.

5.4. *Massive Neutrinos*

Massive neutrinos present particular problems for Fisher matrix analyses of these data sets. Varying the neutrino mass changes the free-streaming scale, below which their rms velocity prevents them from clustering. As Ω_ν (or equivalently m_ν) approaches zero, the neutrinos become fully relativistic and the free-streaming scale of the neutrinos approaches the horizon scale (Bond & Szalay 1983; Holtzman 1989; Ma & Bertschinger 1995; Dodelson, Gates, & Stebbin 1996a; Hu & Eisenstein 1998). This means that at large scales, it takes only a small upward variation of the neutrino mass from zero to bring the neutrinos out of the free-streaming regime. As the power spectra phenomenology differs between these two physical regimes, we expect that the derivative of $P(k)$ or C_l with respect to $\Omega_\nu h^2$ will be

TABLE 4

MARGINALIZED ERRORS FOR VARIOUS COSMOLOGICAL MODELS

	SCDM ($\Omega_B = 0.1$)				OCDM ($\Omega_m = 0.35$)				ΛCDM ($\Omega_m = 0.2$)			
	CMB alone		CMB+SDSS		CMB alone		CMB+SDSS		CMB alone		CMB+SDSS	
QUANTITY	*MAP*	*Planck*	*MAP*	*Planck*	*MAP*	*Planck*	*MAP*	*Planck*	*MAP*	*Planck*	*MAP*	*Planck*
h	0.39	0.16	0.054	0.036	0.34	0.12	0.038	0.021	0.30	0.14	0.028	0.023
Ω_m	1.5	0.64	0.20	0.15	0.36	0.13	0.039	0.023	0.15	0.074	0.015	0.012
$\Omega_m h$	0.38	0.16	0.055	0.038	0.12	0.042	0.021	0.008	0.062	0.030	0.011	0.005
Ω_Λ	1.3	0.55	0.18	0.13	0.75	0.27	0.11	0.052	0.12	0.055	0.021	0.010
Ω_K	0.22	0.090	0.046	0.020	0.39	0.14	0.075	0.029	0.039	0.019	0.010	0.003
$\ln(\Omega_m h^2)$	0.082	0.014	0.076	0.013	0.14	0.011	0.103	0.010	0.097	0.020	0.078	0.015
$\ln(\Omega_B h^2)$	0.044	0.009	0.043	0.008	0.099	0.008	0.055	0.008	0.062	0.011	0.050	0.011
$m_\nu\,(eV) \propto \Omega_\nu h^2$	1.4	0.35	0.68	0.31	0.86	0.15	0.38	0.14	0.59	0.25	0.22	0.15
$n_S(k_{\rm fid})$	0.042	0.008	0.037	0.007	0.075	0.007	0.040	0.006	0.047	0.009	0.038	0.008
α	0.016	0.004	0.015	0.004	0.047	0.004	0.023	0.003	0.027	0.004	0.016	0.004
$\ln P_\Phi(k_{\rm fid}) \equiv \ln A_S^2$	0.38	0.067	0.34	0.066	0.59	0.062	0.35	0.050	0.42	0.077	0.34	0.067
T/S	0.24	0.019	0.22	0.019	0.28	0.016	0.24	0.016	0.13	0.009	0.12	0.009
τ	0.020	0.004	0.020	0.004	0.042	0.005	0.041	0.005	0.025	0.005	0.022	0.004
$\ln\sigma_8$	0.34	0.14	0.101	0.050	0.34	0.056	0.091	0.034	0.17	0.061	0.052	0.036
$\ln(\sigma_{50}/\sigma_8)$	0.42	0.17	0.042	0.034	0.27	0.077	0.038	0.016	0.13	0.076	0.027	0.021
$\ln\beta$	...	...	0.051	0.031	...	...	0.075	0.025	...	...	0.076	0.034
$\ln b$	...	...	0.18	0.12	...	...	0.11	0.053	...	...	0.063	0.047

NOTES.—SCDM model has $\Omega_m = 1$, $\Omega_B = 0.10$, $\Omega_\nu = 0.05$, $\Omega_\Lambda = 0$, $h = 0.5$, and $n_S = 1$. OCDM model has $\Omega_m = 0.35$, $\Omega_B = 0.05$, $\Omega_\nu = 0.0175$, $\Omega_\Lambda = 0$, $h = 0.65$, and $n_S = 1.25$. ΛCDM model has $\Omega_m = 0.2$, $\Omega_B = 0.03$, $\Omega_\nu = 0.01$, $\Omega_\Lambda = 0.8$, $h = 0.8$, and $n_S = 1$. All models have $T/S = 0$, $\tau = 0.05$, $\alpha = 0$, and $Y_p = 0.24$. $n_T = 0$ and cannot vary. All errors are 1 σ. $k_{\rm max} = 0.1\ h\ {\rm Mpc}^{-1}$. CMB experiments include temperature and polarization information.

sharply different above and below this small mass threshold, which is itself a function of scale.

This raises both a practical and a theoretical concern. First, given numerical noise, is it possible to calculate the derivative as Ω_ν goes to zero, or must one always difference pairs of models that bracket the mass transition for some scale of interest? Second, since the derivative is changing significantly even for small values of $\Omega_\nu h^2$, how should we interpret the resulting error bars on $\Omega_\nu h^2$? The difficulty is that the log-likelihood function is not well approximated by a quadratic expansion around $\Omega_\nu = 0$ relative to the quality of the constraints.

This situation is shown in Figure 3. The temperature C_ℓ derivative with respect to the massive neutrino density is a strong function of the fiducial value of Ω_ν. For small Ω_ν, the derivative has a large peak at $\ell \approx 150$, but for larger Ω_ν, the feature goes away entirely. This means that if one began at $\Omega_\nu = 0$ and increased the neutrino mass, the power at $\ell = 150$ would change rapidly at first and then saturate. A Fisher matrix analysis around $\Omega_\nu \approx 0$ would show strong limits on Ω_ν, while an analysis around $\Omega_\nu/\Omega_m \approx 0.2$ would show weak limits.

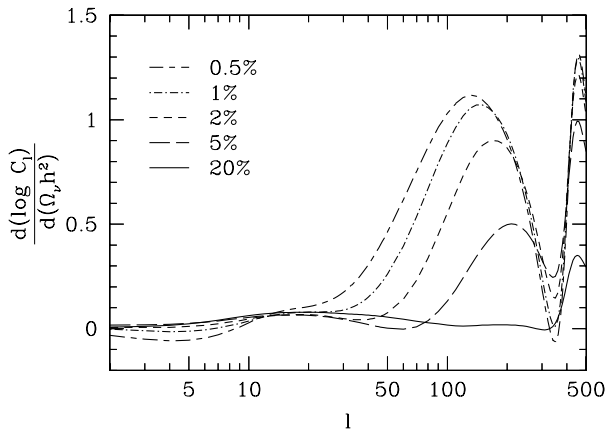

FIG. 3.—Derivative $d(\ln C_{T\ell})/d\Omega_\nu h^2$ as a function of neutrino fraction Ω_ν/Ω_m. *Top to bottom* (for the first peak): 0.5%, 1%, 2%, 5%, and 20%. The cosmology is the $\Omega_m = 0.35$ ΛCDM model, but with $\tau = 0.1$, for a variety of Ω_ν.

The derivative of the matter power spectrum with respect to the neutrino mass shows a similar behavior: it is nonzero only below a break scale that shifts to small k as $\Omega_\nu h^2$ gets smaller. Because of degeneracies, the break itself needs to be detected. Redshift survey data are less restrictive at small k. Hence, whereas CMB data are more restrictive at low Ω_ν, redshift survey data are more restrictive at high Ω_ν.

We are interested in which neutrino masses can be distinguished from zero. Because of the above trend, even if a data set preferred $\Omega_\nu = 0$, the upper limit on the neutrino mass would be underestimated. To be conservative, we use $\Omega_\nu \neq 0$ instead; the significance at which $\Omega_\nu = 0$ can be excluded by the data set is then underestimated.

In Table 5, we present marginalized errors as a function of Ω_ν within a $\Omega_m = 1$ CDM model. *MAP* data alone do not detect the mass of the neutrino in any of the cases. In particular, as Ω_ν increases, the angular scale at which the neutrinos have an observable signature drops below the resolution of the experiment. *Planck* can continue to track the effect and therefore can detect the neutrino mass. In both data sets, as Ω_ν increases, $\Omega_m h^2$ errors tend to decrease, and errors on the tilt sector remain unchanged.

With SDSS data added to *MAP*, neutrino masses exceeding $\sim$1 eV would be detectable (HET). SDSS also improves the limits of *Planck* by up to a factor of 2. Sensitivity to lower masses is possible for $\Omega_m < 1$. Unlike the situation with the ΛCDM models presented elsewhere in this paper, $k_{\rm max} \approx 0.2\ h\ {\rm Mpc}^{-1}$ may be appropriate for the neutrino signatures of SCDM: these models have lower normalization (e.g., cluster abundances suggest $\sigma_8 \approx 0.5$, not 1.0)

TABLE 5

MARGINALIZED ERRORS AS A FUNCTION OF Ω_ν

	$\Omega_\nu = 0.01$ ($m_\nu = 0.24$ eV)			$\Omega_\nu = 0.05$ ($m_\nu = 1.2$ eV)			$\Omega_\nu = 0.10$ ($m_\nu = 2.4$ eV)			$\Omega_\nu = 0.20$ ($m_\nu = 4.7$ eV)		
	CMB	+SDSS		CMB	+SDSS		CMB	+SDSS		CMB	+SDSS	
QUANTITY	T+P	0.1	0.2	T+P	0.1	0.2	T+P	0.1	0.2	T+P	0.1	0.2
MAP:												
$m_\nu\ (eV) \propto \Omega_\nu h^2$	1.1	0.81	0.42	1.4	0.68	0.30	5.5	0.84	0.31	6.8	1.7	0.38
$\ln(\Omega_m h^2)$	0.11	0.101	0.082	0.082	0.076	0.063	0.067	0.065	0.053	0.084	0.059	0.044
h	0.38	0.065	0.020	0.39	0.054	0.018	0.39	0.046	0.017	0.38	0.039	0.015
Ω_m	1.5	0.28	0.092	1.5	0.20	0.068	1.5	0.16	0.055	1.5	0.12	0.039
Planck:												
$m_\nu\ (eV) \propto \Omega_\nu h^2$	0.53	0.47	0.29	0.35	0.31	0.19	0.30	0.28	0.17	0.31	0.31	0.17
$\ln(\Omega_m h^2)$	0.028	0.025	0.018	0.014	0.013	0.011	0.010	0.010	0.010	0.009	0.009	0.009
h	0.16	0.048	0.016	0.16	0.036	0.014	0.16	0.028	0.012	0.16	0.021	0.009
Ω_m	0.64	0.21	0.075	0.64	0.15	0.058	0.64	0.11	0.048	0.64	0.081	0.034

NOTES.—Same ΛCDM model as Table 2, save for variations in Ω_ν. We assume one species of massive neutrino. $n_T = 0$ and does not vary. All errors are 1 σ. All columns include CMB information on temperature and polarization; the top four rows are for *MAP*, and the bottom four for *Planck*. SDSS columns include information to $k_{\max} = 0.1\ h\ \mathrm{Mpc}^{-1}$ or $k_{\max} = 0.2\ h\ \mathrm{Mpc}^{-1}$, as noted.

and thus less nonlinear contamination. Also, because the neutrino signature is not oscillatory, it may be harder for nonlinear dynamics to wash it out.

As Ω_ν increases, performance on Ω_m and h from the combination of SDSS and CMB also improves. Like the baryons, massive neutrinos impress a scale on the matter power spectrum: there is a break in the spectral index around the scale of the horizon at the epoch when the neutrinos become nonrelativistic. This physical scale depends upon $\Omega_m h^2$ and Ω_ν/Ω_m; once these two are determined, one gains leverage on h and Ω_m by detecting the scale in redshift space.

We have used $\Omega_\nu/\Omega_m = 0.05$ unless otherwise specified. With CMB and redshift survey data, this model is distinguished from $\Omega_\nu = 0$ at 2–4 σ. Larger neutrino fractions rely more and more on the matter power spectrum data to provide constraints.

5.5. *Tensors*

Interpreting the errors on the tensor-to-scalar ratio T/S requires special care since we have at present no guide as to its value in the real universe. Although in power-law inflation $T/S \approx 7(1 - n_S)$ (Davis et al. 1992), many inflationary models predict $T/S \approx 0$ (Lyth 1997) and in general slow-roll inflationary models obey $T/S \approx -7n_T$ (see, e.g., Liddle & Lyth 1993). For this reason, we conduct a parameter study of T/S here.

T/S sequence.—As T/S increases in the fiducial model, the errors on most quantities degrade slightly owing to the reduction of small-angle anisotropy signal at fixed *COBE* normalization. With information from SDSS, the degradation is smaller yet. However, the errors on T/S and n_T are strong functions of T/S. Errors on n_T and *fractional* errors on T/S decrease as T/S increases, the latter of course becoming infinite as $T/S \to 0$. Including SDSS information significantly reduces the error bars even in the case of *Planck*; for example, better controlling the value of Ω_Λ and Ω_K substantially helps *Planck* to sort out the various large-angle signals and approach the fixed cosmology limit of Knox (1995) (see also Kinney 1998). We show results for $T/S = 1$, 0.3, and 0.1 in Table 6. Remember, however, that each of these assumes $n_T = 0$ in the fiducial model; the inflationary consistency relation predicts $n_T < 0$ for $T/S \neq 0$, in which case the signal would be slightly overestimated.

T/S-n_T plane.—In the presence of a varying n_T, the value and hence the error bars on the tensor-to-scalar ratio become scale dependent. The ratio of quadrupole power T/S is a pessimistic choice because the ability of the data sets to constrain tensor contributions comes at somewhat smaller angles ($\ell \approx 50$; see also White 1996). Hence, variations in n_T and T/S are highly anticorrelated, and the error bars on T/S do not properly reflect the ability of the experiments to detect the tensor signal. Other choices of parameters, e.g., the ratio of tensor power to scalar power at $\ell = 50$, should yield smaller errors. Appendix A discusses this situation. One can write the general combination of n_T and T/S as $X \equiv T/S + xn_T$. One then varies x to minimize the errors on X. At this minimum, the uncertainties on X are uncorrelated with those on n_T; moreover, the marginalized errors on X (with n_T varying) are identical to those on T/S in the case in which n_T is held fixed. The errors on the best choice of X are shown in Table 6 and better reflect the constraint on the tensor signal.

Detection threshold.—For this set of ΛCDM models, the tensor signal could be detectable with *Planck* at high significance for T/S as low as ~ 0.1 (see Table 6). Only strong tensor signals ($T/S \gtrsim 1$) can be isolated by *MAP*. Redshift survey information can help, especially in case the tensor polarization signal is obscured by foregrounds. Achieving the best performance depends on being able to separate the E and B channels of polarization (Zaldarriaga et al. 1997; Kamionkowski & Kosowsky 1998); for example, if the B channel is completely ignored, then the X errors on the $T/S = 0.1$ model in Table 6 increase by 50%. However, much of the leverage comes from temperature data; if the uncertainty from other large-angle contributors can be removed, the tensor plateau at $\ell \approx 50$ can be detected. For example, as the optical depth in the fiducial model increases, the detection threshold for T/S drops because τ can be better constrained from the temperature data itself (Zaldarriaga et al. 1997).

Consistency relation.—If the tensor-to-scalar ratio approaches unity, the tensor tilt can be measured as well (Knox 1995; Zaldarriaga et al. 1997). This could allow a test

TABLE 6

MARGINALIZED ERRORS AS A FUNCTION OF TENSOR-TO-SCALAR RATIO

	$T/S = 1.0$						
	MAP		*Planck*			$T/S = 0.3$ *Planck*	$T/S = 0.1$ *Planck*
QUANTITY	T+P	SDSS	No B	T+P	SDSS	SDSS	SDSS
T/S	2.0	0.79	0.45	0.42	0.28	0.13	0.064
$X = T/S + xn_T$	0.65	0.54	0.20	0.16	0.14	0.055	0.032
n_T	0.40	0.16	0.12	0.100	0.080	0.14	0.24
$n_S(k_{\rm fid})$	0.065	0.047	0.012	0.012	0.011	0.009	0.008
$n_S(H_0)$	0.45	0.21	0.059	0.055	0.051	0.043	0.040
α	0.048	0.022	0.005	0.005	0.005	0.004	0.004
$\ln P_\Phi(k_{\rm fid}) \equiv \ln A_S^2$	0.59	0.43	0.11	0.103	0.095	0.080	0.074
$\ln P_\Phi(H_0)$	1.4	0.81	0.27	0.25	0.23	0.18	0.17
Value of x	4.9	3.6	3.4	3.7	3.1	0.85	0.23

NOTES.—Same ΛCDM model as Table 2, save for variations in T/S. $n_T = 0$ but can vary. All errors are 1 σ. $k_{\rm max} = 0.1\ h\ {\rm Mpc}^{-1}$. SDSS columns include CMB data with polarization including B channel. The "No B" column presents results in which B-channel polarization has been ignored. The B channel is of negligible importance for *MAP*. x has been chosen so as to minimize the error on the quantity X; for this choice, X is uncorrelated with n_T and the error is equal to the error on T/S if n_T were held fixed. Without CMB polarization information, errors on T/S from the *MAP* or *Planck* are much larger, but errors when combined with SDSS are similar to those in the *MAP* + SDSS column.

of the inflationary prediction $T/S \approx -7n_T$. In attempting to test specific inflationary models, e.g., the $T/S \approx 7(1 - n_S)$ relation of power-law inflation, one should estimate T/S and n_S at the same scale. If $\alpha \neq 0$, the scalar tilt at scales somewhat larger than $k_{\rm fid}$ will be more uncertain that $n_S(k_{\rm fid})$, leading to weaker constraints on inflation.

6. ASSUMPTIONS

6.1. *CMB Foregrounds*

We have assumed that a number of the frequency channels measured by the CMB experiments will be used for foreground removal (e.g., Brandt et al. 1994; Tegmark & Efstathiou 1996; Bersanelli et al. 1996; Tegmark 1998; Hobson et al. 1998), leaving only the subset listed in Table 1 available for cosmology. Assuming that foregrounds can be eliminated to this level may be optimistic, especially for the polarization at the largest angular scales and for small angular scales in general. For the former, the cosmic signal is small (see Fig. 1 [*inset*]) and must be detected against potentially larger Galactic foregrounds (Keating et al. 1997). Large-angle temperature signals are also useful for distinguishing curvature effects but will in any case be severely limited by cosmic variance. On the smallest angular scales, point-source subtraction may be insufficient especially where the cosmic signal is falling owing to the finite duration of last scattering (Toffolatti et al. 1998; Guiderdoni et al. 1998; Tegmark & de Oliveira-Costa 1998; Refregier, Spergel, & Herbig 1998).

If we eliminate even more frequency channels from the Fisher matrix, the errors on cosmological parameters for the model in Table 2 increase only slightly. Restricting *MAP* to use only the 90 GHz channel for temperature data increases errors bars by less than 10%. Using only the 90 GHz channel for both the temperature and the polarization data is a more serious loss: 50% on most parameters and 150% on τ. Essentially, the 90 GHz channel is nearly sample-variance limited for the temperature anisotropies, so little is added by the lower frequencies, while the channels are all roughly equally important for the noise-dominated large-angle polarization signal.

For *Planck*, retaining only the 143 GHz channel for cosmology increases the error bars by ∼10% for temperature only and by ∼15% for temperature and polarization (but 25% on T/S). Retaining only the 217 GHz channel does a little better (∼7%) on temperature and somewhat worse (∼25%) on polarization (and a factor of 3 on T/S). *Planck*'s expected polarization performance does not quite reach the sample-variance limit, but a single channel of temperature data saturates the limit down to a beam scale that varies only slightly between the prime channels.

Conversely, if one adds the channels reserved for foreground subtraction back into the cosmological Fisher matrix, the cosmological error bars do not improve significantly. Even if the remaining eight channels on *Planck* were assumed to give cosmological signal, including them would reduce the temperature-only error bars in Table 2 by only ∼1%! With polarization, errors would decrease by ∼10%, except that T/S errors would shrink by 1.55 because of the artificial assumption that there is no B-polarization sky signal owing to foregrounds, meaning that detector noise always sets the upper limit on that power, no matter how small. *MAP* temperature results are similarly insensitive to the 20 and 30 GHz channels, although the polarization signal can be helped (40% improvement on τ, less on other quantities). Reserving these channels for foreground subtractions thus comes at little cost for cosmology.

6.2. *Gravitational Lensing*

In this paper, we ignore the effects of gravitational lensing on the CMB power spectrum. Gravitational lensing from large-scale structure smooths out the high multipoles of the CMB (Blanchard & Schneider 1987; Cole & Efstathiou 1989; Seljak 1996a) in a way that is dependent on the amplitude of the matter power spectrum at low redshift. Adjusting Ω_Λ and Ω_K to keep a constant angular diameter distance allows large changes in this amplitude thereby breaking the angular diameter distance degeneracy (Metcalf & Silk 1997). However, the effect is small, and even *Planck* cannot use it to attain good estimates on Ω_m and h (Stompor & Efstathiou 1999). We neglect it here since the degeneracy is

broken much more effectively by additional information from redshift surveys or other sources.

6.3. *Varying* $k_{\rm max}$

We have assumed that the galaxy power spectrum follows linear theory on scales longward of a wavenumber $k_{\rm max}$. Nonlinear evolution on smaller scales may obscure the cosmological information in the linear power spectrum. To be conservative, we have neglected all cosmological information on smaller scales.

Baryonic features in the linear power spectrum are of particular importance for cosmological parameter estimation, yet they are washed out at second order in perturbation theory (see, e.g., Jain & Bertschinger 1994). EHT found that fluctuation levels up to $k^3P(k)/2\pi^2 \approx 0.5$ preserved the features for the model of Table 2. Simulations give similar results (Meiksin, Peacock, & White 1998). Hence, for this model, with either CMB or cluster abundance normalization, one may expect linear theory to apply to $k_{\rm max} = 0.1\ h\ {\rm Mpc}^{-1}$ but not much beyond. This is enough to see the first acoustic oscillation.

Because the appropriate value of $k_{\rm max}$ depends on normalization, we show the results for our fiducial ΛCDM model as a function of $k_{\rm max}$ in Table 7. As expected, the results do depend strongly on $k_{\rm max}$. In particular, as $k_{\rm max}$ increases from $0.05\ h\ {\rm Mpc}^{-1}$ to $0.2\ h\ {\rm Mpc}^{-1}$, the errors on h and related quantities drop sharply. In this model, the break in the power spectrum occurs at about $0.03\ h\ {\rm Mpc}^{-1}$, and the first peak is at $0.08\ h\ {\rm Mpc}^{-1}$ (Fig. 2). Little information is added between $k_{\rm max} = 0.2\ h\ {\rm Mpc}^{-1}$ and $k_{\rm max} = 0.4\ h\ {\rm Mpc}^{-1}$ here. On these small scales, the acoustic oscillations have been damped away even in linear theory.

While our choice of $k_{\rm max}$ may be appropriate for baryonic features, other aspects of cosmology may not be so fragile. For example, the broadband level of the linear power spectrum, affected by n_S and α, could potentially be reconstructed from the quasi-linear regime (Peacock & Dodds 1994). As a means of exploring this, we consider an alteration to our treatment of the matter power spectrum, replacing the true linear power spectrum by a smoothed spectrum based on the fitting formula of Eisenstein & Hu (1999). This formula preserves the sharp break at the sound horizon ($k \approx 0.03\ h\ {\rm Mpc}^{-1}$ here) but ignores all the smaller scale oscillations. The resulting marginalized errors are considerably worse, typically equivalent to using the true power spectrum out to $k_{\rm max} \approx 0.05\ h\ {\rm Mpc}^{-1}$. Moreover, the results show little improvement as $k_{\rm max}$ increases from $0.1\ h\ {\rm Mpc}^{-1}$ to $0.4\ h\ {\rm Mpc}^{-1}$. In other words, within the constraints available through CMB satellites, little additional cosmological information is gained by detection of a featureless matter power spectrum. Only detection of the acoustic oscillations or spectral breaks (e.g., massive neutrinos) produces significant improvements. An exception to this conclusion is the error bar on α, the running of the scalar tilt, which continues to improve as $k_{\rm max}$ increases.

6.4. *Smaller Parameter Spaces*

We next consider the effects of removing parameters from our model space. Removing parameters in the face of degeneracies is often motivated by Occam's razor or on the grounds that external information will eliminate some of the options available. In addition, doing so allows us to explore the extent of the degeneracies and facilitates comparison to previous works.

Removing parameters does not require recalculation of models; rather, it means that we hold their value fixed at the fiducial value (by a prior) while the errors on other quantities are computed. In Table 8, we show several different cases, where parameters held fixed are denoted by blank entries, both with and without redshift survey information. The error bars necessarily decrease as degrees of freedom are removed. It is important to remember that improvements found by removing a parameter depend on which the remaining parameters are; in other words, statements such as "removing α is negligible" apply only to the particular context of our 12-dimensional parameter space.

TABLE 7

MARGINALIZED ERRORS AS FUNCTION OF $k_{\rm max}$

		LINEAR $P(k)$				SMOOTH $P(k)$		
QUANTITY	*MAP*	0.05	0.1	0.2	0.4	0.1	0.2	0.4
h	0.22	0.096	0.029	0.012	0.009	0.100	0.089	0.085
Ω_m	0.24	0.098	0.036	0.016	0.014	0.105	0.100	0.099
$\Omega_m h$	0.078	0.033	0.018	0.011	0.009	0.036	0.036	0.036
Ω_Λ	0.19	0.081	0.042	0.024	0.021	0.088	0.087	0.086
Ω_K	0.055	0.030	0.015	0.010	0.009	0.029	0.022	0.020
$\ln(\Omega_m h^2)$	0.095	0.094	0.077	0.054	0.049	0.088	0.071	0.065
$\ln(\Omega_B h^2)$	0.060	0.058	0.050	0.038	0.035	0.058	0.049	0.044
$m_\nu\ (eV) \propto \Omega_\nu h^2$	0.58	0.55	0.33	0.17	0.17	0.43	0.43	0.42
$n_S(k_{\rm fid})$	0.048	0.048	0.040	0.029	0.027	0.045	0.039	0.037
α	0.018	0.018	0.015	0.012	0.007	0.018	0.013	0.008
$\ln P_\Phi(k_{\rm fid}) \equiv \ln A_S^2$	0.43	0.43	0.36	0.26	0.24	0.41	0.35	0.33
T/S	0.18	0.18	0.16	0.14	0.14	0.17	0.17	0.17
τ	0.022	0.022	0.021	0.021	0.021	0.022	0.021	0.021
$\ln\sigma_8$	0.14	0.12	0.070	0.038	0.034	0.12	0.11	0.102
$\ln(\sigma_{50}/\sigma_8)$	0.15	0.066	0.028	0.011	0.010	0.030	0.012	0.011
$\ln\beta$	...	0.090	0.068	0.053	0.045	0.094	0.093	0.091
$\ln b$	...	0.22	0.087	0.041	0.035	0.24	0.22	0.21

NOTES.—Same ΛCDM model as Table 2. $n_T = 0$ and cannot vary. All errors are 1 σ. CMB data for *MAP* with temperature and polarization information included on all columns. Linear $P(k)$ means using actual linear power spectrum. Smooth $P(k)$ columns use a fitting formula that captures the break at the sound horizon but eliminates the baryon oscillations in $P(k)$.

TABLE 8

MARGINALIZED ERRORS AS FUNCTION OF PARAMETER SPACE

Quantity	*MAP* (TP)							*MAP* + SDSS						
h	0.22	0.22	0.064	0.052	0.063	0.048	0.022	0.029	0.029	0.024	0.014	0.024	0.014	0.012
Ω_m	0.24	0.23	0.098	0.081	0.097	0.074	0.034	0.036	0.034	0.036	0.020	0.036	0.019	0.016
$\Omega_m h$	0.078	0.076	0.042	0.035	0.041	0.031	0.015	0.018	0.015	0.015	0.008	0.015	0.008	0.007
Ω_Λ	0.19	0.18	0.098	0.081	0.097	0.074	0.034	0.042	0.035	0.036	0.020	0.036	0.019	0.016
Ω_K	0.055	0.054	...	...	...	...	...	0.015	0.012	...	...	...	...	...
$\ln(\Omega_m h^2)$	0.095	0.069	0.086	0.073	0.084	0.065	0.035	0.077	0.059	0.033	0.020	0.033	0.018	0.018
$\ln(\Omega_B h^2)$	0.060	0.042	0.055	0.054	0.053	0.050	0.025	0.050	0.035	0.028	0.028	0.028	0.028	0.023
$m_\nu\,(eV) \propto \Omega_\nu h^2$	0.58	0.53	0.58	...	0.56	...	...	0.33	0.30	0.31	...	0.31	...	...
Y_P	0.020	0.020	0.020	...	0.020	...	...	0.020	0.020	0.020	...	0.020	...	...
$n_S(k_{\rm fid})$	0.048	0.028	0.045	0.039	0.045	0.037	0.014	0.040	0.024	0.021	0.018	0.021	0.018	0.012
$n_S(H_0)$	0.17	0.15	0.16	0.14	0.045	0.037	0.014	0.14	0.12	0.14	0.14	0.021	0.018	0.012
α	0.018	0.018	0.016	0.016	...	...	...	0.015	0.014	0.014	0.014	...	...	...
$\ln P_\Phi(k_{\rm fid}) \equiv \ln A_S^2$	0.43	0.25	0.40	0.35	0.40	0.34	0.12	0.36	0.21	0.18	0.15	0.18	0.15	0.101
$\ln P_\Phi(H_0)$	0.71	0.29	0.71	0.57	0.61	0.51	0.18	0.61	0.23	0.49	0.46	0.27	0.24	0.15
T/S	0.18	...	0.17	0.16	0.16	0.15	...	0.16	...	0.12	0.12	0.087	0.085	...
τ	0.022	0.021	0.022	0.021	0.021	0.020	0.020	0.021	0.020	0.021	0.021	0.020	0.020	0.020
$\ln \sigma_8$	0.14	0.14	0.13	0.056	0.12	0.052	0.035	0.070	0.069	0.062	0.027	0.062	0.027	0.027
$\ln(\sigma_{50}/\sigma_8)$	0.15	0.15	0.074	0.059	0.069	0.057	0.033	0.028	0.028	0.027	0.017	0.027	0.015	0.015
$\ln \beta$	...	...	...	...	...	...	...	0.068	0.058	0.047	0.046	0.045	0.043	0.038
$\ln b$	...	...	...	...	...	...	...	0.087	0.087	0.082	0.031	0.080	0.031	0.029

NOTES.—Same ΛCDM model as Table 2. $n_T = 0$ and cannot vary. All errors are 1 σ. CMB data for *MAP* with temperature and polarization information included on all columns. SDSS columns use CMB data and $k_{\rm max} = 0.1\ h\ {\rm Mpc}^{-1}$. Blank entries indicate that the parameter has been held fixed.

Tensors.—Eliminating tensors from the model (i.e., assuming $T/S = 0$) allows n_S, $\Omega_m h^2$, and $\Omega_B h^2$ to be determined better by *MAP*. *Planck*'s longer lever arm allows it to constrain n_S regardless of tensors.

Curvature.—Fixing the curvature of course breaks the angular diameter distance degeneracy by assumption. Therefore, CMB data alone can turn the location of the acoustic peaks into a measure of h, Ω_m, and other quantities. It is interesting to note, however, that *MAP* does not get enough accuracy on, e.g., $\Omega_m h^2$ to keep uncertainties in the sound horizon from propagating into the measure of the angular diameter distance. *Planck* without polarization does only slightly better in this regard.

If SDSS information is included, assuming $\Omega_K = 0$ makes very little difference to errors on h and Ω_m, since the angular distance degeneracy is already broken. It does, however, affect other parameters that determine the peak locations such as $\Omega_B h^2$, $\Omega_m h^2$, and $n_S(k_{\rm fid})$. To see why this is so, consider the general case in which Ω_K is allowed to vary. One has two uncertain quantities, Ω_Λ and Ω_K, to map a fairly well-constrained quantity, the sound horizon, to the location of the peaks in C_ℓ and $P(k)$. This yields good constraints on Ω_Λ and Ω_K. Now, with $\Omega_K = 0$ assumed, these two observations can both constrain Ω_Λ *and* reduce the remaining uncertainties on the sound horizon. Hence, we see that assuming $\Omega_K = 0$ reduces error bars on $\Omega_m h^2$, $\Omega_B h^2$, and $n_S(k_{\rm fid})$.

Neutrinos and helium.—Removing $\Omega_\nu h^2$ and Y_P from the $\Omega_K = 0$ case makes further small improvements. Y_P affects the ionization history and free electron density so as to change the sound horizon and damping length. $\Omega_\nu h^2$ is partially degenerate with $\Omega_m h^2$.

Running of the tilt.—Removing α makes very little difference except on quantities that depend on extrapolating the initial power spectrum beyond the well-observed range, e.g., $n_S(H_0)$ and A_S^2 (see also Copeland et al. 1998). As discussed in § 3, with α free, the spectral tilt becomes scale dependent, but there exists a scale at which the error on the tilt is unchanged by the removal of α. From the fact that the errors in Table 8 on $n_S(k_{\rm fid})$ change very little as α is removed, one can infer that $k_{\rm fid} = 0.025\ {\rm Mpc}^{-1}$ is close to this "pivot point." With SDSS information, removing α helps to better determine T/S.

Combined.—For *MAP* alone, removing tensors on top of removing Ω_K, $\Omega_\nu h^2$, Y_P, and α makes a significant difference (compare the last two columns of the *MAP*-only section of Table 8). Apparently, combinations of parameters were conspiring to hide their effects at $\ell < 100$.

In short, stripping the parameter space down to a minimum of baryons, CDM, cosmological constant, and tilt (with τ and A_S^2 controlling the normalization) makes a factor of 3 difference in the error bars from *MAP* even for parameters that are not associated with strong degeneracies. Including SDSS reduces this dependence; in fact, *MAP* plus SDSS in the general parameter space with only curvature fixed performs as well as *MAP* alone in this minimal parameter space! Degenerate parameters are of course affected much more strongly.

7. CONSISTENCY

Even if the CMB does end up spinning a seamless tale of structure formation and cosmological parameters, it will not spell the end of cosmology. Only with stringent consistency checks from other types of cosmological data can we be confident that we have eliminated systematic effects in the data and its analysis. Moreover, parameter estimation is only as good as its underlying parameter space; testing CMB conclusions against other cosmological probes is an important way to search for unrecognized physical effects.

One of the most important data sets for this task is the galaxy power spectrum from redshift surveys. While we have focused in this paper on the ways in which such surveys can complement CMB data to improve parameter estimation, this has assumed that the measured power spec-

trum is consistent with the locus of allowed models from the CMB. In fact, with the precision of upcoming surveys, this is not guaranteed: there are many possible spectra that will simply be inconsistent with our understanding of cosmology from the CMB. Attributing the discrepancy to nonlinear clustering or galaxy bias has consequences that are testable within the survey data; it is not clear that the discrepancy will be resolved in favor of the CMB. Explanations involving alterations to the dark matter sector (see, e.g., Turner & White 1997; Caldwell, Dave, & Steinhardt 1998; Hu 1998 for recent suggestions) could severely modify the implications of the CMB for both low-redshift cosmology and particle physics.

It is also possible that CMB data and the matter power spectrum will tell a consistent story, while the true nature of the universe is subtly otherwise, which causes other cosmological measurements to differ from predictions. Exotic late-time equations of state for smooth components are an example of this situation (Huey et al. 1999). Therefore, in the following, we consider consistency checks with other cosmological data sets.

7.1. H_0, Ω_m, and Acceleration

A rich area for consistency checks is the sector of classical cosmology: $H_0, \Omega_m, \Omega_\Lambda$ (and implicitly $\Omega_K = 1 - \Omega_m - \Omega_\Lambda$). As explained above, CMB anisotropies suffer from a severe degeneracy here, but a large variety of other precision measurements are available to clarify the ambiguity and provide consistency checks. There are a number of candidates: the matter power spectrum, Type Ia supernovae (Perlmutter et al. 1998; Riess et al. 1998), and direct measures of H_0 (see, e.g., Freedman et al. 1998; Blandford & Kundic 1996; Cooray et al. 1998) seem particularly promising. Figures 4 and 5 show how the combination of each of these with CMB data yields a small region in parameter space. The

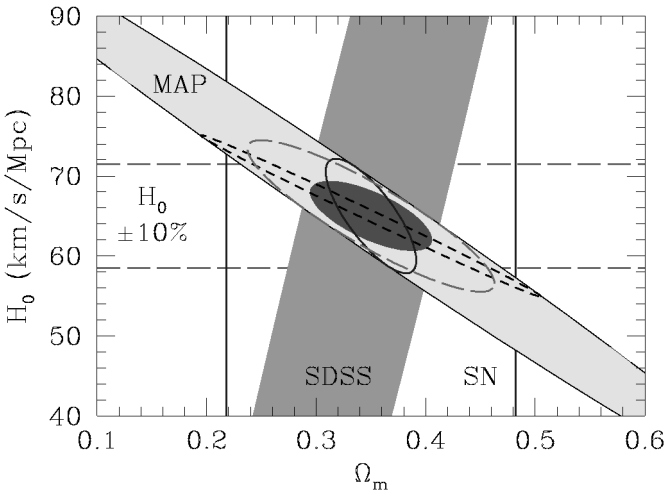

FIG. 4.—Constraint regions in the Ω_m-h plane from various combinations of data sets. *MAP* data with polarization yield the ellipse from upper left to lower right, assuming the universe flat yields a small region (*short-dashed line*). SDSS ($k_{max} = 0.1\ h\ \mathrm{Mpc}^{-1}$) gives the vertical shaded region; SDSS combined with *MAP* gives the small filled ellipse. A projection of future Type Ia supernova results (Tegmark et al. 1998a, *middle prediction*) gives the solid vertical lines as bounds; combining this with *MAP* yields the solid ellipse. A direct 10% measurement of H_0 gives the long-dashed lines and ellipse. All regions are 68% confidence. For a two-dimensional elliptical Gaussian, this contour is at 1.52 σ. For a one-dimensional Gaussian, the contour is the usual 1 σ; the curves for H_0 alone, SDSS alone, and supernovae alone are treated as one-dimensional. The fiducial model is the $\Omega_m = 0.35$ ΛCDM model from Table 2.

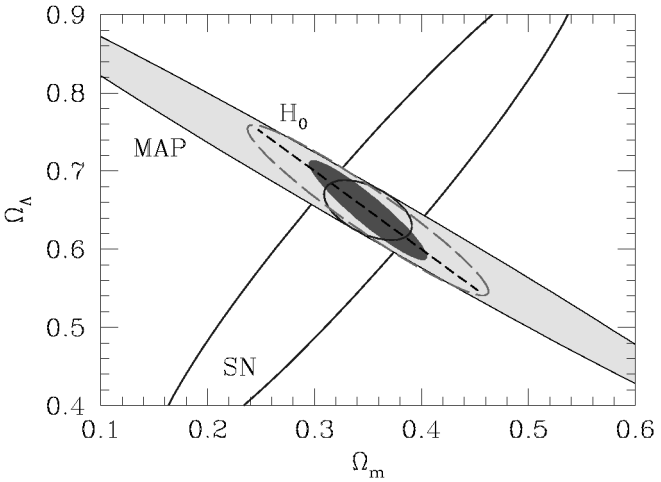

FIG. 5.—As Fig. 4, but for constraints in the Ω_m-Ω_Λ plane. Lines and shadings are unchanged in meaning. In this projection, the assumption that the universe is flat (*short-dashed line*) yields a line, not an ellipse (cf. Fig. 4). We therefore calculate this 68% confidence region as if it were one-dimensional. SDSS-only constraints are not shown.

overlap of these three regions would be a highly nontrivial test of cosmology. Direct measurements of Ω_m, for example from M/L (see, e.g., Carlberg et al. 1997b) or cluster evolution (see, e.g., Carlberg et al. 1997a; Bahcall et al. 1997), would also be powerful, and constraints on Ω_Λ from gravitational lensing (see, e.g., Kochanek 1996) provide a consistency test. In viewing the two-dimensional projections in Figures 4 and 5, one should remember that error region from a combination of data sets is not simply the intersection of the individual two-dimensional error regions. These figures are projections of the 12-dimensional parameter space, and complementary information in the hidden dimensions can cause the combined error regions to be substantially smaller than would be suggested by the two-dimensional intersection.

If the smooth component of missing energy is more complicated than a cosmological constant or curvature, then the constraints from CMB plus the galaxy power spectrum can still be compared to results from classical H_0 programs. However, the supernovae then yield a measurement of this exotic equation of state (Garnavich et al. 1998; Hu et al. 1999)!

7.2. *Normalization, Reionization, and Bias*

Another fruitful area for consistency checks involve parameters associated with the amplitude of fluctuations in the CMB and galaxy power spectrum.

Several sources of ambiguity in the interpretation of the relative amplitudes today should be resolved with the larger dynamic range of upcoming CMB and galaxy data sets. Tensors affect the *COBE* normalization and the spectral tilt adjusts its extrapolation to smaller scales, but the new satellites will focus on smaller angular scales for a direct comparison to the scales probed in redshift surveys. Massive neutrinos affect the matter power spectrum far greater than the CMB and hence change the relative normalization between these two. Fortunately, they should also have detectable signatures (see § 5.4).

Within our parameter space, there are three remaining factors that alter the observed relative amplitude of the

CMB anisotropies and the galaxy power spectrum. First, the growth factor between recombination and the present day depends upon Ω_Λ and Ω_K. Second, galaxy bias alters the normalization of the galaxy power spectrum relative to that of the matter (and CMB). Third, reionization suppresses CMB anisotropies for a given level of potential fluctuations.

Because the addition of redshift survey information breaks the angular distance degeneracy, the growth factor will be accurately known. As discussed in the previous section, there are many consistency checks to ensure the validity of this statement.

This leaves the bias and reionization optical depth strongly covariant, as shown in Figure 6. Without polarization information to determine τ and other dynamical measurements to determine b, neither will be well determined.

With a polarization detection of the large-angle reionization signal, however, the error bars on τ plummet, yielding b and σ_8 to $\sim 5\%$ fractionally. Because polarization measurements are subject to many systematic effects, consistency checks here are particularly important. With Ω_m measured precisely, any means of constraining β or σ_8 will provide a consistency check on this measurement, e.g. redshift distortions (see Hamilton 1997 for a review), peculiar velocity catalogs (Strauss & Willick 1995 and references within), and cluster abundances (White et al. 1993a; Viana & Liddle 1996; Eke et al. 1996; Pen 1998). Additionally, if these measurements can produce limits on β or below the values given in the tables ($\lesssim 5\%$), then this extra information can provide leverage on other parameters such as h and $\Omega_m h^2$ once τ has been fixed by the polarization detection. On the other hand, if large-angle CMB foregrounds prevent us from extracting the reionization signal, precision measures of b or σ_8 would sharply constrain τ.

A measurement of the optical depth to last scattering may yield an additional consistency test, in that it requires the cosmological model to ionize the universe at some particular redshift. If this redshift is uncomfortably high or low, it may challenge our cosmological assumptions, for example, the extrapolation of $P_\Phi(k)$ to yet smaller scales.

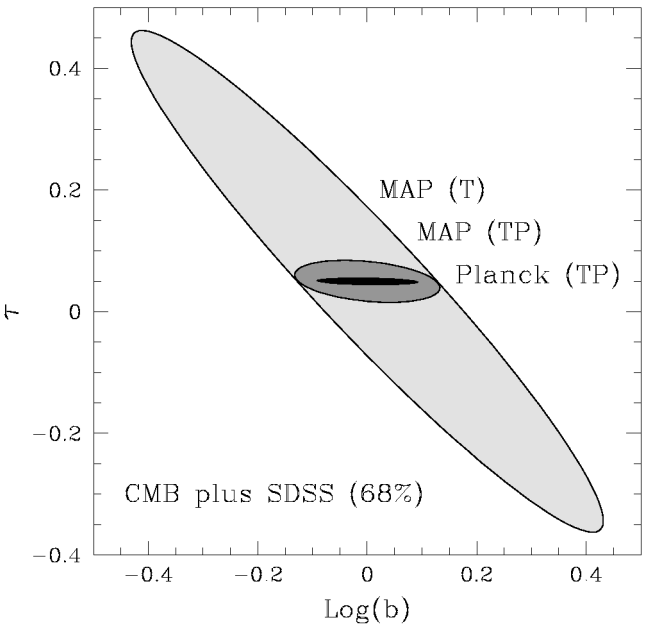

FIG. 6.—Allowed region in the b-τ plane for the ΛCDM model from Table 2. The 68% confidence region is shown for *MAP*+SDSS, with and without polarization, and *Planck*+SDSS, with polarization. $k_{\max} = 0.1\ h\ \mathrm{Mpc}^{-1}$.

8. CONCLUSION

We have presented Fisher matrix calculations of the cosmological information obtainable with upcoming CMB satellite missions and large redshift surveys. We have used a considerably larger parameterization of adiabatic CDM than previous works involving polarization data or redshift surveys. Within this space, we have conducted several parameter studies, including variations in Ω_B, Ω_ν, and T/S. In a number of cases, we find stronger degeneracies and hence larger errors bars than prior work. We attribute these discrepancies to artificially broken degeneracies caused by numerical subtleties such as use of one-sided derivatives and overly large step sizes.

The primary purpose of this paper has been to explore the ways in which galaxy power spectrum data can provide complementary information to the CMB, thereby significantly reducing error bars. In the language of degeneracies, we seek places in which large-scale structure offers the means to break CMB degeneracies and vice versa. The most important example of this is the angular-diameter distance degeneracy of the CMB, which causes uncertainty on h, Ω_m, Ω_Λ, and even σ_8. The presence of baryonic oscillations in matter power spectrum offers a robust way to break this degeneracy. Redshift survey data also help determine the mass of the heaviest neutrino, especially if it exceeds 1 eV. Although the projections of the *Planck* satellite with polarization suffice to do most everything else, less sensitive CMB experiments can benefit from redshift surveys even on measuring quantities such as $\Omega_m h^2$ and $\Omega_B h^2$.

While CMB and galaxy power spectra themselves offer a myriad of consistency tests, they also provide a baseline for tests against other cosmological measurements. With the detection of the large-angle polarization signal due to reionization, the two data sets together yield a $\sim 5\%$ measure of linear galaxy bias, to be compared to that obtained from peculiar-velocity and redshift-distortion methods. Similarly, supernovae distance measurements and Hubble constant measurements provide a fertile set of cross-checks on the breaking of the angular diameter distance degeneracy.

It is important to remember that the error estimates presented here reflect the statistical leverage available within these data sets. We have not attempted to produce a data analysis pipeline that would address the horde of obstacles that stand between the raw data and these cosmological inferences. Considerable effort has been channeled toward the development of such methods. Foreground removal was mentioned in § 6.1. Pipeline methods have been developed and implemented for CMB mapmaking (Wright 1996; Wright, Hinshaw, & Bennett 1996; Tegmark 1997b), CMB power spectrum extraction (Tegmark 1997c; Bond, Jaffe, & Knox 1998; Oh, Spergel, & Hinshaw 1999) and galaxy power spectrum estimation (Tegmark et al. 1998b). All of these are lossless in the sense that they retain all the cosmological information quantified by the Fisher information matrix, but it is likely that many aspects of the problem will only be revealed once the data are in hand. Approaching the performance described by analyses such as those in this paper will be one of the primary goals (and motivations for) of all this hard work!

In summary, while CMB satellite missions can provide marvelous cosmological information, they do not make other methods obsolete. Additional precision measurements will be needed both to break the parameter degeneracies of the CMB and to test for consistency in the face of systematic errors and additional physical effects. Only with these precise comparisons can one build a secure cosmological model.

Numerical power spectra were generated with CMBfast by Uros Seljak and Matias Zaldarriaga.[7] We thank Martin White for supplying his results on parameter estimation for comparison. We thank Arthur Kosowsky, Andrew Liddle, David Spergel, Yun Wang, Martin White, and Matias Zaldarriaga for useful discussions. D. J. E. is supported by a Frank and Peggy Taplin Membership at the IAS, W. H. by the W. M. Keck Foundation, and D. J. E. and W. H. by NSF-9513835. M. T. was supported by NASA through grant NAG5-6034 and Hubble Fellowship HF-01084.01-96A from STScI, operated by AURA, Inc. under NASA contract NAS4-26555.

[7] http://arcturus.mit.edu/~matiasz/CMBFAST/cmbfast.html.

APPENDIX A

MINIMIZING ERRORS BY REDUCING COVARIANCE

At several points in the paper, we are concerned with how the uncertainties on a particular quantity depend upon the uncertainties on other related quantities with which it is correlated. Here we show that a particular linear combination of the correlated quantities has the minimum variance and is uncorrelated with the other parameters. This variance is furthermore equal to that of the original quantity under the assumption that the correlated parameters have been fixed by priors. We examine optimal combinations of the scalar tilt n_S and running of the tilt α as examples. The case of the tensor-scalar ratio T/S and tensor tilt n_T was discussed in § 5.5.

A1. PROOF

We assume an n-dimensional parameter space with independent variables $p_1, \ldots, p_n$. Let the primary quantity be p_1 and the $m-1$ quantities ($m \le n$) that we want to combine be $p_2, \ldots, p_m$. We seek a new quantity $X = f(p_1, p_2, \ldots, p_m)$ that has $\partial f/\partial p_1 = 1$ and minimum errors. The former requirement is to prevent simple rescalings of the variable p_1; X and p_1 will in this sense have the same scale.

In the Fisher matrix formalism, all that matters is the gradient of X with respect to the independent variables. We write $w_j = \partial f/\partial p_j$ and arrange them as a vector $\boldsymbol{w}$; by construction, $w_1 = 1$ and $w_j = 0$ for $m < j \le n$. Then the smallest attainable variance of X will be

$$\sigma_X^2 = \boldsymbol{w}^T C \boldsymbol{w} , \tag{A1}$$

where C is the inverse of the Fisher matrix F. We seek the set of $w_2, \ldots, w_m$ that minimize σ_X^2. Clearly only the submatrix $\tilde{C}$ involving the first m rows and columns of C can be involved. Using Lagrange multipliers, one readily shows that the minimum is achieved at

$$w_j = \begin{cases} \dfrac{(\tilde{C}^{-1})_{1j}}{(\tilde{C}^{-1})_{11}} & j \le m , \\ 0 & m < j \le n . \end{cases} \tag{A2}$$

The minimum value of σ_X^2 is then $(\tilde{C}^{-1})_{11}^{-1}$.

If one replaces the independent variable p_1 by X, then the transformed matrix C will have $C_{1j} = 0$ for $j = 2, \ldots, m$. In other words, X is uncorrelated with the variables $p_2, \ldots, p_m$. This means that X will have the same errors regardless of whether $p_2, \ldots, p_m$ vary or are held fixed. If they are held fixed, then X and p_1 are locally identical. Hence, the error on X with $p_2, \ldots, p_m$ varying is the same as the error of p_1 with them held fixed.

Note that in the case of $m = n$, $\tilde{C}^{-1} = F$. Hence, $\boldsymbol{w}$ is just the renormalized first column of the Fisher matrix, and the minimum variance of X is simply $1/F_{11}$. Aficionados will recognize this as the variance of p_1 if all other variables are held fixed.

In the case of $m = 2$, where we wish to combine p_1 with one other variable p_2, we obtain the special case that $X = p_1 - p_2 C_{12}/C_{22}$ and $\sigma_X^2 = C_{11} - C_{12}^2/C_{22}$. X and p_2 are uncorrelated.

A2. A TILT EXAMPLE

An interesting example of this concerns n_S and α. We define our independent variable to be $n_S(k_{\rm fid})$ and α. For most values of $k_{\rm fid}$, these two will be correlated. What is special in this case is that the minimum-error combination X is a physically motivated quantity, namely the tilt n_S at some new scale $k_{\rm pivot} = k_{\rm fid} \exp(-C_{n_S\alpha}/C_{\alpha\alpha})$ (see eq. [15]). As shown above, $n_S(k_{\rm pivot})$ is uncorrelated with α and has the same error with α varying as n_S on any scale would have if α were held fixed.

The pivot scale $k_{\rm pivot}$ at which the error on $n_S(k_{\rm pivot})$ is minimized depends on the experiment and on the fiducial model. For our ΛCDM model and SDSS alone, $k_{\rm pivot}$ is 0.024 Mpc^{-1} (0.088 Mpc^{-1}) for $k_{\rm max} = 0.1\ h$ Mpc^{-1} (0.2 h Mpc^{-1}). For CMB data (with SDSS to 0.1 h Mpc^{-1} in parentheses), the scales in Mpc^{-1} are 0.034 (0.036) for *MAP*(T), 0.018 (0.020) for *MAP*(TP), 0.084 (0.070) for *Planck*(T), and 0.029 (0.027) for *Planck*(TP). As expected, *Planck* adds more small-scale sensitivity, while polarization adds more large-scale sensitivity by resolving the low-ℓ degeneracies. Our choice of $k_{\rm fid} = 0.025$ Mpc^{-1} is close to the desired spot, and the errors grow only to second order in $\ln(k)$ away from the minimum:

$$\sigma^2_{n_S(k)} = \sigma^2_{n_S(k_{\rm pivot})} + \ln^2(k/k_{\rm pivot})\sigma^2_\alpha\ . \tag{A3}$$

APPENDIX B

NUMERICAL METHODS

B1. DERIVATIVE METHODOLOGY

As described in § 2, the calculation of the Fisher matrix reduces to manipulation of derivatives of the various power spectra with respect to cosmological parameters. However, the near cancellation of certain linear combinations of derivatives leaves the Fisher matrix nearly singular. As the larger error bars are themselves inverses of the smaller eigenvalues, it is critical to prevent numerical effects from perturbing these small eigenvalues. Hence, constructing and manipulating the derivatives requires care, lest a parameter degeneracy be broken by numerical effects and yield an overestimate of the experiment's ability to measure the associated parameters. We find that our treatment of certain derivatives reveals significantly softer directions in parameter space than found by previous works (see Appendix C). Therefore, we will describe our methods in some detail.

B1.1. *Two-sided Derivatives*

Wherever possible, we take two-sided derivatives. Writing $f(p)$ for the dependence of either $\ln C_\ell$ or $\ln P(k)$ on some parameter p with all others fixed, this means that we approximate $f'(p)$ by

$$\tilde{f}'(p) \equiv \frac{f(p+\Delta p) - f(p-\Delta p)}{2\Delta p} \tag{B1}$$

for some small step size Δp. This is exact to second order in Δp, whereas approximating $f'(p)$ with the one-sided difference $[f(p+\Delta p) - f(p)]/\Delta p \approx f'(p+\Delta p/2)$ is only good to first order; moreover, the latter corresponds to an accurate estimate of the derivative at a slightly shifted parameter value $p + \Delta p/2$. This is critical when perturbing parameters that change the locations of the Doppler peaks because the various derivatives will no longer be in phase! If the step size is sufficiently large, these phase shifts will break the parameter degeneracies.

One also should avoid differencing models that are calculated with different numerical techniques, as these can cause discontinuous results as one adjusts the independent variable. With CMBfast v2.3.2, this situation occurs for geometrically flat versus open models and for models with differing numbers of species of massive neutrinos.

Because of the desire to use two-sided derivatives, we take nonzero fiducial values for nonnegative quantities such as $\tau = 0.05$ and $\Omega_\nu/\Omega_m = 0.05$ unless otherwise noted. Perturbing around $\Omega_\nu \neq 0$ also allows us to use one species of massive neutrinos in all cases.

TABLE 9

LIST OF INDEPENDENT PARAMETERS

Quantity	Step Size	Notes
$\Omega_m h^2$	$\pm 5\%$	
$\Omega_B h^2$	$\pm 5\%$	
$\Omega_\nu h^2$	$\pm 10\%$	Equivalent to m_ν
Ω_Λ	$\pm 0.05\Omega_m$	
Ω_K	$\Delta\Omega_m = -0.1\Omega_m$	See § B2.1
τ	± 0.02	
Y_p	± 0.02	Prior of ± 0.02
$n_S(k_{\rm fid})$.....	± 0.005	See eq. (14)
α	± 0.005	See eq. (14)
T/S	Exact	
n_T	± 0.01	Only if $T/S \neq 0$.
A_S^2	Exact	
β	Exact	$\equiv \Omega_m^{0.6}/b$

NOTES.—Step sizes are for our ΛCDM model; those listed as percentages are fractions of the fiducial value.

B1.2. *Derivative Step Sizes*

What is the best choice of the step size Δp for constructing the derivative in equation (B1)? We use CMBfast v2.3.2 (including the bug fixes of v2.4.1; Seljak & Zaldarriaga 1996; Zaldarriaga & Seljak 1997) for our numerical derivatives and find that this version of CMBfast has random numerical noise at a level of $\sigma \equiv \delta C_\ell/C_\ell \sim 10^{-4}$ for geometrically flat models and 10^{-3} for open models.[8] As described by Press et al. (1992), the optimal compromise between numerical noise and higher order Taylor series terms occurs for $\Delta p \sim \sigma^{1/3} p_c$, where p_c indicates the characteristic scale on which p varies. Hence, if $p_c \sim p$, we should use fractional steps of roughly 5%, yielding an accuracy of $\sim$0.2%. Note that a one-sided derivative with a 5% step would yield a truncation-dominated accuracy of $\sim$5%, which is considerably worse.

Since this estimate is quite crude, we performed a series of numerical experiments with different step sizes before arriving at the choices in listed in Table 9. We have tested that our answers change by less than 10% when using half the listed steps. Convergence is better as degeneracies are lifted by complementary information or by reducing the parameter space via priors. Only for the open fiducial model do we see some lack of convergence owing mainly to the larger noise associated with open models. The step sizes on n_S, n_T, and α could easily have been significantly smaller, although reducing them to 10^{-4} changes the marginalized errors by less than 1%.

B2. CURVATURE

Curvature is known to be strongly degenerate with other effects, such as a cosmological constant, that alter the late-time evolution of the universe (Hu & Sugiyama 1995, § VI.B2; Bond et al. 1997; Zaldarriaga et al. 1997). Combinations of changes in these parameters that hold the angular diameter distance to last scattering fixed will leave the acoustic peaks unchanged (given a proper choice of normalization). Differences in the decay of potentials at late times will alter the large-angle anisotropy; this alteration of the ISW effect is the primary way to break this degeneracy in the absence of lensing effects (Hu et al. 1997; Stompor & Efstathiou 1999).

When faced with a strong degeneracy, it is numerically desirable to change variables in parameter space by introducing a parameter in the degenerate direction. This has the advantage of containing all numerical problems in a single (very small) derivative, where the physical effects can be easily understood and distinguished from numerical errors making the derivative artificially large. We adopt this approach for the angular distance degeneracy, as detailed in the following three subsections.

B2.1. *Differentiating with d_A Fixed*

Including variations in curvature around a flat model presents a particular concern because no closed version of CMBfast is available. Hence, the derivative with respect to curvature is necessarily a one-sided derivative. Moreover, the open version of the code is noisier than the flat, which forces one to take larger step sizes for the derivatives. Since adding curvature causes a significant shift in the location of the CMB peaks, large step sizes cause the curvature derivative to be out of phase with the Ω_Λ derivative. This is displayed in Figure 7; the dashed line in the bottom panel shows that the two derivatives in the top panel cannot be exactly cancelled.

We work around this problem by altering our coordinate basis so that the only derivative in a direction with nonzero curvature has a convenient physical property. The derivative of Ω_Λ at constant Ω_K may be done in the usual manner. But for the derivative of Ω_K at constant Ω_Λ, we transform to the basis of Ω_K and angular diameter distance d_A. The latter is defined as

$$d_A = \frac{1}{\sqrt{\Omega_K H_0^2}} \sinh\left[\sqrt{\Omega_K}\int_0^{z_*} \frac{dz}{\sqrt{E(z)}}\right]$$
$$E(z) = \Omega_\Lambda + \Omega_K(1+z)^2 + \Omega_m(1+z)^3 + \Omega_R(1+z)^4\,, \tag{B2}$$

where Ω_R is the density of radiation and z_* is the redshift of recombination (Hu & White 1997a). We treat massive neutrinos according to the approximation of Appendix A of Hu & Eisenstein (1998). The desired curvature derivative is then

$$\left(\frac{\partial}{\partial\Omega_K}\right)_{\Omega_\Lambda} = \left(\frac{\partial}{\partial\Omega_K}\right)_{d_A} + \frac{(\partial d_A/\partial\Omega_K)_{\Omega_\Lambda}}{(\partial d_A/\partial\Omega_\Lambda)_{\Omega_K}}\left(\frac{\partial}{\partial\Omega_\Lambda}\right)_{\Omega_K}. \tag{B3}$$

In flat models, the first term is constructed by a one-sided finite difference in curvature corresponding to $\Delta\Omega_m = -0.1\Omega_m$. The second term consists of a numerical prefactor times the derivative that we have already calculated. The first term is special because with the proper choice of normalization it is a derivative in the direction of constant Doppler peak location, shape, and height. This means that aside from an ISW signal at low ℓ and lensing effects at high ℓ, the derivative vanishes, which allows one to isolate the numerical noise. Also, since the peak structure of both derivatives enters through the same $\partial/\partial\Omega_\Lambda$ at constant Ω_K term, the two derivatives are guaranteed to cancel up to the treatment of the first term of equation (B3).

B2.2. *Differentiating with Fixed High-z Normalization*

To properly implement the technique of the last section, one must choose a normalization convention that is independent of Ω_Λ and Ω_K. This condition is satisfied by keeping unchanged the physical situation at high redshift. It is implemented by

[8] This does not apply to variations in the initial power spectrum, as the anisotropies generated by different wavenumbers are weighted and combined at double precision. The quoted levels are for $\ell \lesssim 100$ and may increase beyond that.

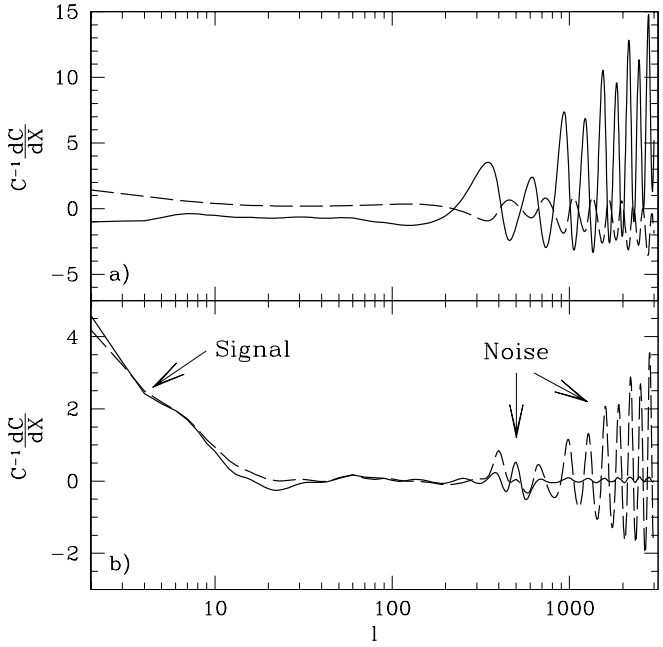

FIG. 7.—(*a*) Derivatives of $C_{T\ell}$ with respect to Ω_K at constant Ω_Λ (*solid line*) and with respect to Ω_Λ at constant Ω_K (*dashed line*). The former is a one-sided derivative formed by differencing models with $\Omega_K = 0.01$ and $\Omega_K = 0.003$. (*b*) Derivative of $C_{T\ell}$ with respect to Ω_K at constant d_A, constructed in two different ways. *Solid line*: result from differencing two models with Ω_Λ and Ω_K altered so as to keep d_A fixed. *Dashed line*: the appropriate linear combination of the curves in (*a*); the poor cancellation is due to the curvature derivative being one-sided and therefore out of phase. The glitch at $\ell \approx 500$ in the solid curve is numerical noise and the reason we need to truncate this derivative.

holding fixed the amplitude of the scalar gravitational potential at high redshift on some comoving reference scale $k_{\rm norm}$ in Mpc^{-1} that is outside the horizon at the redshift in question. We use the low-redshift growth function to shift the scalar potential back to the pure-matter–domination phase (ignoring radiation). This produces the normalization

$$P(k_{\rm norm}, z = 0) = A_S^2 \left(\frac{k_{\rm norm}}{k_{\rm fid}}\right)\left(1 + \frac{3\Omega_K H_0^2}{k_{\rm norm}^2}\right)^2 H_0^{-4} c^4 D_{\rm gr}^2 \ ; \tag{B4}$$

($n_S = 1$) in other words, we choose A_S^2 as an independent variable and therefore renormalize the calculated (*COBE* normalized) $P(k)$ and C_ℓ by equation (B4) to hold A_S^2 constant when taking all other derivatives. Here $D_{\rm gr}$ is the growth function integral (Peebles 1980)

$$D_{\rm gr} = \frac{5}{2}\int_0^1 \frac{a^{3/2}\, da}{(\Omega_m + \Omega_K a + \Omega_\Lambda a^3)^{3/2}} \ . \tag{B5}$$

Note that in the Harrison-Zeldovich case, the normalization is independent of $k_{\rm norm}$ in the large-scale limit; we choose a normalization scale of $k_{\rm norm}^{-1} = 3000$ Mpc. If $n_S \neq 1$, it is important to pick $k_{\rm norm}$ to be independent of h. Since the high-redshift ratios of the various types of matter and radiation are held fixed when perturbing Ω_Λ and Ω_K, it does not matter whether we normalize to the matter-domination or radiation-domination potential.

B2.3. *Noise Clipping*

Even with the derivative technique of the last two sections, the numerical noise of CMBfast v2.3.2 breaks the angular diameter distance degeneracy. Fortunately, with this choice of derivatives, the true signal is well localized in ℓ. Neglecting gravitational lensing (see § 6.2), the only signal in the curvature derivative at constant d_A is the low-ℓ ISW effect. This effect scales as $C_\ell \sim \ell^{n_S - 4}$ asymptotically (Hu & White 1996).

Since the goal of our analysis is to make robust and conservative estimates for how accurately cosmological parameters can be measured, we assume that no useful cosmological information can be extracted from lensing effects or from ISW contributions at large ℓ. For $\ell > \ell_{\rm clip} = 30$, we therefore set $C'_\ell = (\ell_{\rm clip}/\ell)^{4-n_S} C'_{\ell_{\rm clip}}$ for this particular derivative, thereby throwing away all of the high-ℓ numerical noise that would otherwise artificially break the degeneracy above some ℓ-cutoff $\ell_{\rm clip}$. This numerical noise is displayed as the solid line in Figure 7; the glitches at $\ell \approx 500$ dominate the breaking of the degeneracy for either satellite.

Hence, while our error bars on Ω_Λ and Ω_K for *Planck* alone (especially with polarization) are overestimated owing to the neglect of lensing, we protect the small eigenvalue of this degeneracy against the numerical problems that would otherwise dominate.

B2.4. *Effects of* Ω_K *and* Ω_Λ *on* $P(k)$

Ω_K and Ω_Λ have degenerate effects on $P(k)$ as well, and so we must take care in constructing these derivatives. Fortunately, there is an analytic solution. The matter power spectrum can be decomposed into an initial power spectrum whose time dependence reflects only the physics on the largest scales times a transfer function that incorporates the effects of causal physics (see, e.g., Eisenstein & Hu 1998, 1999). Ω_K and Ω_Λ shift the $z = 0$ normalization of the initial power spectrum relative to the level of CMB anisotropies by altering the growth function $D_{\rm gr}$ (eq. [B5]). Meanwhile, the transfer function is independent of Ω_K and Ω_Λ if it is measured in real space instead of redshift space. Hence, Ω_K and Ω_Λ enter this piece only through their effect on h. We can rewrite this as a derivative with respect to k:

$$\frac{d\ln P}{d\Omega_K} = 2\frac{d\ln D_{\rm gr}}{d\Omega_K} - \frac{1.2}{\Omega_m} + \frac{1}{2\Omega_m}\left(\frac{d\ln P}{d\ln k} - 1\right). \tag{B6}$$

This avoids having to difference two different Boltzmann code outputs and allows us to track the oscillations in the power spectrum and its derivative more accurately. The middle term in equation (B6) comes from the derivative of $\ln b$, since β is our independent variable. The derivative with respect to Ω_Λ has an equivalent formula. The assumption that the transfer function in real space is independent of Ω_K and Ω_Λ is actually violated slightly at small scales if massive neutrinos are important due to differences in the infall of the neutrinos (Hu & Eisenstein 1998); we ignore this effect as it is tiny and primarily beyond the linear regime.

B3. τ AND NORMALIZATION

Reionization mimics a suppression of the amplitude of the primary CMB anisotropies on all but the largest scales. For small optical depths, the secondary fluctuations generated by these late-time scatterings are small because only a small fraction of photons are affected and because the scattering occurs over a sufficient range of distances along the line of sight that small-scale perturbations are averaged out (Kaiser 1984). Hence, for $\tau \ll 1$, the main effect is a suppression of C_ℓ by $\exp(-2\tau)$ for all but the lowest ℓ. If the normalization of the primary fluctuations is unknown, then we can hide the reionization simply by increasing their normalization by a corresponding amount. The resulting degeneracy is difficult to break in the temperature anisotropy data because the rise at low ℓ up to the original fluctuation level is hidden by cosmic variance. With polarization data, reionization can be more easily separated because it produces a bump at large angles whereas fluctuations at high redshift cannot produce much large-angle polarization due to causality (Kaiser 1983).

With this level of degeneracy, one should worry about artificially breaking the cancellation between the τ and A_S^2 derivatives. However, we find that CMBfast is sufficiently accurate to track this degeneracy without invoking tricks similar to those used for the curvature, e.g., differentiating with $A_S e^{-\tau}$ held fixed.

Note that if our chosen normalization were the *COBE* normalization, we would also have to worry about degeneracies between the tensor-to-scalar ratio T/S and the scalar normalization. By normalizing to the scalar potential fluctuations, however, we avoid this problem.

APPENDIX C

COMPARISON TO PREVIOUS WORK

The results in the main part of this paper are not directly comparable to those of previous papers owing to differences in parameter spaces or fiducial models. In this Appendix, we attempt to provide as direct a comparison as we can for some of the results presented in these papers. We have in all cases matched the quoted parameter spaces and experimental specifications. Except in the case of White (1999), we have not taken care to provide an exact match to the normalization in these comparisons. All groups are normalizing to the *COBE* value for the signal-to-noise ratio in equation (11). While normalization differences of a few percent are possible, these would not affect the parameter results beyond this small level.

In Table 10, we compare marginalized errors with Bond et al. (1997) for their standard CDM model. We use their experimental specifications for *MAP* and the *Planck* High-Frequency Instrument HFI (temperature only) and restrict ourselves to their parameter space ($\Omega_K = \alpha = 0$). Note that we have by necessity used one-sided derivatives for τ and Ω_ν differencing models with 0.01 and 0.001 in each parameter. Because the curvature is not varied, the tricks of § B2 are not needed. We find significantly (up to a factor of 3) larger errors on some parameters.

Zaldarriaga et al. (1997) analyzed a standard CDM model with a smaller parameter space. Restricting to this space ($\Omega_K = \Omega_\nu = \alpha = \Delta Y_P = 0$) and adopting their specifications for *MAP* yields the results in Table 11. Because $\tau \neq 0$ and massive neutrinos are excluded, no one-sided derivatives are required. The results agree well with temperature and polarization data (except for n_S) but can be up to a factor of 2 different with temperature data alone.

We suspect that the numerical issues addressed in Appendix B1 are responsible for discrepancies described above. Unfortunately, based on the published information, we cannot confirm in the above cases that this is the source of the discrepancies.

Our comparison with Wang et al. (1999) demonstrates the situation. We compared two fiducial models, adopting their parameter space ($\Omega_K = \alpha = \Omega_\nu = T/S = \Delta Y_P = 0$) and specifications for *MAP* (with $f_{\rm sky} = 0.8$). At first, agreement was poor, with their errors being as much as a factor of 5 smaller on one model. One-sided derivatives had been used; when Wang et al.

TABLE 10

COMPARISON TO BOND ET AL. (1997)

	MAP		*Planck* (HFI)	
QUANTITY	BET	EHT	BET	EHT
$2h$	0.19	0.40	0.02	0.08
$4\Omega_\Lambda h^2$	0.49	1.2	0.05	0.20
$\ln \Omega_B h^2$	0.09	0.14	0.006	0.018
$4\Omega_m h^2$	0.18	0.38	0.02	0.04
$4\Omega_\nu h^2$	0.07	0.09	0.02	0.03
n_S	0.06	0.10	0.006	0.015
T/S	0.38	0.69	0.09	0.11
τ	0.22	0.34	0.16	0.30
$\ln \sigma_8$	0.28	0.57	0.18	0.33

NOTES.—Fiducial model has $\Omega_m = 1$, $h = 0.5$, $\Omega_B = 0.05$, $\Omega_\nu = 0$, $\Omega_\Lambda = 0$, $\tau = 0$, $n_S = 1$, $T/S = 0$, and $Y_P = 0.23$ (with a prior of $\Delta Y_P = 0.02$. All errors are 1 σ. BET columns contain the errors quoted in Bond et al. 1997; EHT columns contain the errors we find using their experimental specifications for *MAP* and the High-Frequency Instrument (HFI) of *Planck*. All columns are temperature data only.

(1999) kindly recomputed their results using two-sided derivatives and smaller steps on certain parameters, the agreement became quite good ($\lesssim$20%), as shown in Table 12. We did not compare results for SDSS and CMB together because the treatments are quite different: they remove baryon oscillations from $P(k)$ and apply a nonlinear evolution correction.

In another situation in which we could confirm that two-sided derivatives were used, we have attained even better agreement. We have compared a ΛCDM model with the preliminary results of White (1999), who uses a hierarchy Boltzmann code rather than CMBfast. Under a parameter space of $\Omega_B h^2$, $\Omega_m h^2$, Ω_Λ, τ, n_S, and A_S^2, the marginalized error bars agree to 3% with and without polarization for *MAP* and *Planck*. Adding Ω_K causes larger discrepancies, mostly along the direction of the angular diameter distance degeneracy; we suspect the hierarchy code is more stable for $\Omega_K \neq 0$, but the differences should disappear once the degeneracy is broken by outside information.

Degeneracies are quite important even in these smaller parameter spaces. As an example, consider the SCDM model from Zaldarriaga et al. (1997). Holding τ fixed removes the reionization-normalization degeneracy and leaves $\Omega_m h^2$, $\Omega_B h^2$, Ω_Λ, n_S, T/S, and A_S^2 to vary. This set of parameters in this fiducial model can be combined to cancel the normalization temperature derivative to better than 1 part in 100 over the ℓ-range 100–800, mostly through a combination of tilt, tensors, and $\Omega_m h^2$.

TABLE 11

COMPARISON TO ZALDARRIAGA ET AL. (1997)

	MAP(T)		*MAP*(TP)	
QUANTITY	ZSS	EHT	ZSS	EHT
T/S Variable:				
h	0.092	0.17	0.051	0.040
Ω_Λ	0.53	1.1	0.29	0.25
$\Omega_B h^2$	0.0010	0.0019	0.00061	0.00055
τ	0.13	0.21	0.021	0.022
n_S	0.059	0.12	0.031	0.028
T/S	0.39	0.77	0.22	0.19
T/S Fixed:				
h	0.017	0.025	0.016	0.017
Ω_Λ	0.098	0.15	0.093	0.103
$\Omega_B h^2$	0.00030	0.00043	0.00028	0.00035
τ	0.12	0.15	0.021	0.021
n_S	0.0098	0.021	0.0048	0.010
T/S	...	...	...	...

NOTES.—Fiducial model has $\Omega_m = 1$, $h = 0.5$, $\Omega_B = 0.05$, $\tau = 0.05$, $n_S = 1$, and $T/S = 0$. Ω_K, Ω_ν, Y_P, and α are held fixed. The top set of numbers is with T/S allowed to vary; the bottom set is with T/S fixed. All errors are 1 σ. ZSS columns contain the errors quoted in Zaldarriaga et al. 1997; EHT columns contain the errors we find using their experimental specifications for *MAP* with and without polarization.

TABLE 12

COMPARISON TO WANG ET AL. (1999)

		MAP(T)		*MAP*(TP)	
MODEL	QUANTITY	WSS	EHT	WSS	EHT
SCDM	$\ln h$	0.052	0.051	0.033	0.033
	Ω_Λ	0.15	0.15	0.091	0.097
	$\ln \Omega_B h^2$	0.028	0.031	0.020	0.024
	$\ln \tau$	2.4	2.9	0.39	0.38
	n_S	0.017	0.020	0.0085	0.0090
ΛCDM.....	$\ln h$	0.066	0.077	0.032	0.035
	$\ln \Omega_\Lambda$	0.076	0.089	0.037	0.043
	$\ln \Omega_B h^2$	0.044	0.052	0.021	0.023
	$\ln \tau$	1.3	1.6	0.18	0.18
	n_S	0.035	0.041	0.014	0.014

NOTES.—Top set of numbers are for a standard CDM fiducial model with $\Omega_m = 1$, $h = 0.5$, $\Omega_B = 0.05$, $\tau = 0.05$, and $n_S = 1$. Bottom set are for a ΛCDM model with $\Omega_m = 0.3$, $h = 0.65$, $\Omega_B = 0.06$, $\Omega_\Lambda = 0.7$, $\tau = 0.1$, and $n_S = 1$. Ω_K, Ω_ν, Y_P, T/S, and α are held fixed. All errors are 1 σ. WSS columns contain the errors quoted in the revised version of Wang et al. (1999; private communication). EHT columns contain the errors we find using their experimental specifications for *MAP* with and without polarization.

Hence, even in this small space, one needs to control the derivatives to high numerical accuracy. For example, a 0.05 one-sided step in tilt pivoting around the Hubble distance produces a 16% derivative error at $\ell \approx 600$ owing to second-order terms. These considerations and the comparison with Wang et al. (1999) and White (1999) lead us to conclude that two-sided derivatives are crucial for achieving accurate answers with present-day codes.

REFERENCES

Bahcall, N. A., Fan, X., & Cen, R. 1997, ApJ, 485, L53
Bersanelli, M., et al. 1996, *COBRAS/SAMBA*, Phase A Study for an ESA M3 Mission, ESA Report D/SCI(96)3
Blanchard, A., & Schneider, J. 1987, A&A, 184, 1
Blandford, R. D., & Kundic, T. 1996, in The Extragalactic Distance Scale, ed. M. Livio, M. Donahue, & N. Panagia (Cambridge: Cambridge Univ. Press), 60
Blumenthal, G., et al. 1984, Nature, 311, 517
Bond, J. R., Crittenden, R., Davis, R. L., Efstathiou, G., & Steinhardt, P. J. 1994, Phys. Rev. Lett., 72, 13
Bond, J. R., Efstathiou, G., & Tegmark, M. 1997, MNRAS, 291, L33
Bond, J. R., & Jaffe, A. H. 1997, in Microwave Background Anisotropies, ed. F. Bouchet et al. (Gif-sur-Yvette: Editions Frontières), 197
Bond, J. R., Jaffe, A. H., & Knox, L. 1998, Phys. Rev. D, 2117, 1998
Bond, J. R., & Szalay, A. S. 1983, ApJ, 274, 443
Brandt, W. N., et al. 1994, ApJ, 424, 1
Bunn, E. F., & White, M. 1997, ApJ, 480, 6
Caldwell, R. R., Dave, R., & Steinhardt, P. J. 1998, Phys. Rev. Lett., 80, 1582
Carlberg, R. G., Morris, S. L., Yee, H. K. C., & Ellingson, E. 1997a, ApJ, 479, L19
Carlberg, R. G., Yee, H. K. C., & Ellingson, E. 1997b, ApJ, 478, 462
Cole, S., & Efstathiou, G. 1989, MNRAS, 239, 195
Coles, P. 1993, MNRAS, 262, 1065
Cooray, A. R., Carlstrom, J. E., Joy, M. Grego, L., Holzapfel, W., & Patel, S. K. 1998, preprint [astro-ph/9804149]
Copeland, E. J., Grivell, I. J., & Liddle, A. R. 1998, MNRAS, 298, 1233
David, L. P., Jones, C., & Forman, W. 1995, ApJ, 445, 578
Davis, R. L., Hodges, H. M., Smoot, G. F., Steinhardt, P. J., & Turner, M. S. 1992, Phys. Rev. Lett., 69, 1856
Dodelson, S., Gates, E., & Stebbins, A. 1996a, ApJ, 467, 10
Dodelson, S., Gates, E., & Turner, M. S. 1996b, Science, 274, 69
Efstathiou, G., & Bond, J. R. 1999, MNRAS, 304, 75
Eisenstein, D. J., & Hu, W. 1998, ApJ, 496, 605
———. 1999b, ApJ, 511, 5
Eisenstein, D. J., Hu, W., & Tegmark, M. 1998, ApJ, 504, L57 (EHT)
Eke, V. R., Cole, S., & Frenk, C. S. 1996, MNRAS, 282, 263
Evrard, A. E. 1997, MNRAS, 292, 289
Freedman, W. L., Mould, J. R., Kennicutt, R. C., & Madore, B. F. 1998, in IAU Symp. 183, Cosmological Parameters and the Evolution of the Universe, ed. K. Sato (Dordrecht: Kluwer), in press
Fry, J. N., & Gaztañaga, E. 1993, ApJ, 413, 447
Garnavich, P., et al. 1998, ApJ, 509. 74
Gawiser, E., & Silk, J. 1998, Science, 280, 1405
Goldberg, D. M., & Strauss, M. 1998, ApJ, 495, 29
Guiderdoni, B., Hivon, E., Bouchet, F. R., & Maffei, B. 1998, MNRAS, 295, 877
Hamilton, A. J. S. 1997, in Ringberg Workshop on Large-Scale Structure, ed. D. Hamilton (Dordrecht: Kluwer), 185
Hatton, S. J., & Cole, S. 1998, MNRAS, 296, 10
Heavens, A. F., & Taylor, A. N. 1997, MNRAS, 290, 456
Hobson, M. P., Jones, A. W., Lasenby, A. N., & Bouchet, F. R. 1998, MNRAS, 300, 1
Holtzman, J. A. 1989, ApJS, 71, 1
Hu, W. 1998, ApJ, 506, 485
Hu, W., & Eisenstein, D. J. 1998, ApJ, 498, 497
Hu, W., Eisenstein, D. J., & Tegmark, M. 1998, Phys. Rev. Lett., 80, 5255 (HET)
Hu, W., Eisenstein, D. J., Tegmark, M., & White, M. 1999, Phys. Rev. D, 59, 023512
Hu, W., & Sugiyama, N. 1995, Phys. Rev. D, 51, 2599
———. 1996, ApJ, 471, 542
Hu, W., Sugiyama, N., & Silk, J. 1997, Nature, 386, 37
Hu, W., & White, M. 1996, M. A&A, 315, 33
———. 1997a, ApJ, 479, 568
———. 1997b, NewA, 2, 323
Huey, G., Wang, L., Dave, R., Caldwell, R. R., & Steinhardt, P. J. 1999, Phys. Rev. D, 59, 063008
Jain, B., & Bertschinger, E. 1994, ApJ, 431, 495
Jungman, G., Kamionkowski, M., Kosowsky, A., & Spergel, D. N. 1996a, Phys. Rev. Lett., 76, 1007
———. 1996b, Phys. Rev. D, 54, 1332
Kaiser, N. 1983, MNRAS, 202, 1169
———. 1984, ApJ, 282, 374
Kaiser, N., & Peacock, J. A. 1991, ApJ, 379, 482
Kamionkowski, M., & Kosowsky, A. 1998, Phys. Rev. D, 57, 685
Kamionkowski, M., Kosowsky, A., & Stebbins, A. 1997, Phys. Rev. Lett., 78, 2058
Keating, B., Timbie, P., Polnarev, A., & Steinberger, J. 1998, ApJ, 495, 580
Kinney, W. H. 1998, Phys. Rev. D, in press
Knox, L. 1995, Phys. Rev. D, 52, 4307
Kochanek, C. S. 1996, ApJ, 466, 638
Liddle, A. R., & Lyth, D. H. 1993, Phys. Rep., 231, 1
Lineweaver, C. H. 1998, ApJ, 505, L69
Lyth, D. H. 1997, Phys. Rev. Lett., 78, 1861
Ma, C. P., & Bertschinger, E. 1995, ApJ, 455, 7
Mann, R. G., Peacock, J. A., & Heavens, A. F. 1998, MNRAS, 293, 209
Meiksin, A., Peacock, J. A., & White, M. 1998, MNRAS, in press
Metcalf, R. B., & Silk, J. 1997, ApJ, 489, 1
Oh, S. P., Spergel, D. N. & Hinshaw, G. 1999, ApJ, 510, 551

Peacock, J. A. 1997, MNRAS, 284, 885
Peacock, J. A., & Dodds, S. J. 1994, MNRAS, 267, 1020
Peebles, P. J. E. 1980, The Large-Scale Structure of the Universe (Princeton: Princeton Univ. Press)
Peebles, P. J. E., & Yu, J. T. 1970, ApJ, 162, 815
Pen, U.-L. 1998, ApJ, 468, 30
Perlmutter, S., et al. 1998, Nature, 391, 51
Press, W. H., Teukolsky, S. A., Vetterling, W. T., & Flannery, B. P. 1992, Numerical Recipes (2d ed.; Cambridge: Cambridge Univ. Press)
Refregier, A., Spergel, D. N., & Herbig, T. 1998, ApJ, submitted [astro-ph/9806349]
Riess, A. G., et al. 1998, AJ, 116, 1009
Scherrer, R. J., & Weinberg, D. H. 1998, ApJ, 504, 607
Schramm, D. N., & Turner, M. S. 1998, Rev. Mod. Phys., 70, 303
Scott, D., Silk, J., & White, M. 1995, Science, 268, 829
Scott, D., Srednicki, M., & White, M. 1994, ApJ, 421, L5
Seljak, U. 1996a, ApJ, 463, 1
———. 1996b, ApJ, 482, 6
Seljak, U., & Zaldarriaga, M. 1996, ApJ, 469, 437
Stompor, R., & Efstathiou, G. 1999, MNRAS, 302, 735
Strauss, M., & Willick, J. 1995, Phys. Rep., 261, 271
Sunyaev, R., & Zeldovich, Ya. B. 1970, Ap&SS, 7, 3
Tegmark, M. 1997a, Phys. Rev. Lett., 79, 3806
———. 1997b, ApJ, 480, L87
———. 1997c, Phys. Rev. D, 55, 5895
———. 1998, ApJ, 502, 1
Tegmark, M., & de Oliveira-Costa, A. 1998, ApJ, 500, 83
Tegmark, M., & Efstathiou, G. 1996, MNRAS, 281, 1292
Tegmark, M., Eisenstein, D. J., Hu, W., & Kron, R. 1998a, preprint [astro-ph/9805117]
Tegmark, M., Hamilton, A. J. S., Strauss, M. A., Vogeley, M. A., & Szalay, A. S. 1998b, ApJ, 499, 555
Tegmark, M., Taylor, A. N., & Heavens, A. F. 1997, ApJ, 480, 22
Toffolatti, L., Argueso Gomez, F., De Zotti, G., Mazzei, P., Franceschini, A., Danese, L., & Burigana, C. 1998, MNRAS, 297, 11
Turner, M. S., & White, M. 1996, Phys. Rev. D, 53, 6822
———. 1997, Phys. Rev. D, 56, 4439
Viana, P. T. P., & Liddle, A. R. 1996, MNRAS, 281, 323
Wang, Y., Spergel, D. N., & Strauss, M. A. 1999, ApJ, 510, 20
Webster, M., Hobson, M. P., Lasenby, A. N., Hahav, O., & Rocha, G. 1998, ApJ, submitted [astro-ph/9802109]
Weinberg, D. H. 1995, in Wide-Field Spectroscopy and the Distant Universe, ed. S. J. Maddox & A. Aragón-Salamanca (Singapore: World Scientific), 129
Weinberg, D. H., Miralda-Escudé, J., Hernquist, L., & Katz, N. 1997, ApJ, 490, 564
White, D. A., & Fabian, A. C. 1995, MNRAS, 273, 72
White, S. D. M., Efstathiou, G., & Frenk, C. S. 1993a, MNRAS, 262, 1023
White, S. D. M., Navarro, J. F., Evrard, A. E., & Frenk, C. S. 1993b, Nature, 366, 429
White, M. 1996, Phys. Rev. D, 53, 3011
———. 1999, in preparation
Wright, E. L. 1996, unpublished [astro-ph/9612006]
Wright, E. L., Hinshaw, G., & Bennett, C. L. 1996, ApJ, 458, L53
Zaldarriaga, M., & Seljak, U. 1997, Phys. Rev. D, 55, 1830
Zaldarriaga, M., Spergel, D. N., & Seljak, U. 1997, ApJ, 488, 1